Results and perspectives in dark photon physics

- M. RAGGI(1)(*) and V. KOZHUHAROV(1)(2)(**)
- (1) INFN, Laboratori Nazionali di Frascati Frascati (RM), Italy
- (2) University of Sofia "St. Kl. Ohridski" Sofia, Bulgaria

received 21 July 2015

Summary. — The introduction of a hidden sector of particles and a new very weak interaction with the fundamental Standard Model fermions could explain the anomalies in the muon magnetic moment, the results from scattering experiments searching for Dark Matter and also the antimatter excess in the cosmic rays. The simplest interaction scenario is an additional U(1) gauge symmetry resembling the electromagnetism but with a massive interaction carrier —the dark photon A'. Such a model has a high predictive power and is being extensively tested by past and present experiments. Present status of the dark photon searches is discussed as well as the possible improvements in the near future.

```
PACS 12.60.Cn - Extensions of electroweak gauge sector.
```

PACS 13.40.Em - Electric and magnetic moments.

PACS 95.35.+d - Dark matter (stellar, interstellar, galactic, and cosmological).

```
450
         1.
             Introduction
452
              Dark sector primer
453
              2.1. Dark photon models
453
                    2.1.1. Kinetic mixing
455
                    2^{\cdot}1.2.
                            B-L
456
                    2^{\circ}1.3.
                            Leptophilic gauge boson
                    2.1.4.
457
                            Flavour non-universal coupling
              2.2. Dark photon mass generation
458
              2.3. Dark photon production
459
              Anomalous magnetic moment
461
462
              3.1. Dark photons and (g_e - 2)
464
                   Muon anomalous magnetic moment
              3.2.
              Experimental search for the dark photons
465
                   Visible decay search techniques
465
```

^(*) E-mail: mauro.raggi@lnf.infn.it

^(**) E-mail: venelin.kozhuharov@cern.ch

```
466
                     4.1.1.
                             Dump experiments
                     4.1.2.
471
                             Meson decay experiments
471
                     4.1.3.
                             Searches for dark photon at KLOE
473
                             WASA at COsy
                     4.1.4.
473
                     4^{\circ}1.5.
                             HADES at GSI
474
                     4.1.6.
                             Searches for dark photon at BaBar
                     4.1.7.
                             Dark photon in \pi^0 decays by NA48/2
475
475
                     4.1.8.
                             Dark photon searches in heavy ion collisions
476
              4.2.
                     Fixed-target experiments
                             APEX test run
476
                     4.2.1.
                     4.2.2.
                             A1 experiment at MAMI
478
478
              4.3.
                    Invisible decay search techniques
480
                     4.3.1.
                             Dark matter scattering searches
                     4.3.2.
                             Searches for the dark photon at MiniBooNe
481
481
                     4.3.3.
                             Missing-mass-based searches
                     4.3.4.
                             Indirect limits
483
483
              Future dark photon searches
         5
483
                     Experiments devoted to visible dark photon decays
483
                     5.1.1.
                             The HPS experiment
                     5.1.2.
                             MAMI and MESA
486
486
                     5.1.3.
                             PADME dump at LNF
487
                     5.1.4.
                             NA62 at CERN
487
                     5.1.5.
                             Mu3e at PSI
488
              5.2.
                    Searches sensitive to invisible decays
488
                     5.2.1.
                             VEPP3
                     5^{\circ}2.2.
                             PADME at LNF
489
491
                     5.2.3.
                             DarkLight experiment
                     5.2.4.
                             Cornell
491
492
                     5^{\circ}2.5.
                             BDX at JLAB
                     5.2.6.
                             P348
494
                             Belle II at KEK
496
                     5^{\circ}2.7.
496
                     5.2.8.
                             SHiP at CERN
              Constraints for non-minimal dark photon models
498
498
                     Searches through Higgs portal at LHC
498
                     6.1.1.
                             Search for dark photon at ATLAS
499
                     6.1.2.
                             Search for dark photon at CMS
500
              6.2.
                     Searches for dark Higgs
500
                     6.2.1.
                             Search for dark Higgs at BaBar
501
                     6.2.2.
                             Search for dark Higgs at Belle
501
                     6.2.3.
                             Search for dark Higgs at KLOE
503
              Conclusions and discussion
         7.
```

1. - Introduction

The discovery of the Higgs boson [1,2] underlined the success of the Standard Model (SM) as a theory describing the interactions among the known fundamental particles. However there are few phenomena which indicate that the Standard Model is just a low energy approximation of another more fundamental theory.

Dark matter (DM) is responsible for the missing mass in the Universe and is about five times more abundant than the ordinary barionic matter [3]. It cannot be incorporated within the Standard Model and its possible understanding requires the introduction of new, weakly interacting with the ordinary matter, degrees of freedom.

Recently the measurement of the antiproton spectrum in the cosmic rays performed by the AMS Collaboration [4] provided an additional evidence that antimatter in the cosmic rays is not just due to secondary production. This result together with the positron excess in the cosmic rays observed earlier by PAMELA [5] and confirmed by FERMI [6] and AMS [7] could be interpreted as products of the annihilation of dark matter particles. The annihilation could lead to the production of an interaction carrier which consequently decays into Standard Model particles.

The direct searches for Weakly Interacting Massive Particles (WIMPs) also provided signals which could indicate that the Dark matter interacts with the ordinary matter. An excess of events of unknown origin has been reported by both DAMA/LIBRA [8] and CoGeNT [9] experiments. In addition, a modulation of this excess was observed with period consistent with one year and a phase leading to a maximum at $t_{\rm max}=102\pm47$ days and $t_{\rm max}=136\pm7$ days (from January, 1st) correspondingly for CoGeNT and DAMA/LIBRA. The preferred region of parameters clusters towards WIMPs mass of order of $O(5\,{\rm GeV})$. The mechanism of the WIMPs scattering could involve an interaction carrier of approximately arbitrary mass.

Another issue in the low energy particle physics is the long standing discrepancy between the measured and the calculated anomalous magnetic moment of the muon — $a_{\mu} = (g_{\mu} - 2)/2$

$$a_{\mu}^{\text{SM}} = 116591802(2)(42)(26) \times 10^{-11},$$
 (1)
$$a_{\mu}^{\text{exp}} = 116592091(54)(33) \times 10^{-11}.$$

The difference between the Standard Model prediction [10] and the experimental result [11], $\Delta a_{\mu} = a_{\mu}^{\rm exp} - a_{\mu}^{\rm SM} = 289(63)(49) \times 10^{-11}$, is more than three standard deviations away from zero. This discrepancy can indicate lepton flavour non-universality (or violation) since it relates the electromagnetic coupling constant determined mostly from the anomalous magnetic moment of the electron a_e with the a_{μ} and is a result of the description of the two observables with a single interaction constant. A solution to that problem could be due to the New Physics (NP) effect, in which "a relatively light hypothetical vector boson from the dark matter sector that couples to our world of particle physics [12]". The preferred mass region lies in the interval $M_V \sim 10$ –100 MeV.

The explanation of any of the described phenomena requires introduction of physics beyond the Standard Model. One of the possible directions is the introduction of new particles with masses high enough and certainly above the threshold we have reached so far. However even with the present highest energy reached at the colliders no indication of New Physics has been observed. On the other hand it is the so-called precision physics that requires high statistics and/or high intensity approach. The mentioned discrepancies do not point towards the necessity to introduce short distance effects. They could well be explained by the introduction of states that are almost decoupled from the Standard Model particles, so called *hidden sector*. The mass scale of the hidden sector could be arbitrary as long as its interaction with the SM particles is weak. Thus one can actually represent the New Physics contribution as a combination of two terms —ultraviolet (UV), responsible for the new high mass degrees of freedom and suppressed by the UV scale Λ_{UV} , and a long distance infrared (IR) contribution [13]

(2)
$$\mathcal{L} = \mathcal{L}_{SM} + \mathcal{L}_{NP}$$
, where $\mathcal{L}_{NP} = \mathcal{L}_{UV} + \mathcal{L}_{IR}$.

Numerous experimental results published recently probe the infrared extension of the Standard Model and the results in this direction are reviewed here.

2. - Dark sector primer

The most general low energy extension of the Standard Model is so-called dark sector due to its extremely weak interaction with the known sector. The dark sector could consist of rich phenomenology and states. The connection between the standard sector and the dark sector is usually done through a mediator —a particle which possesses both Standard Model and dark sector quantum numbers. Alternatively the Standard Model fields could interact with the mediator either directly, if they possess charge under the newly introduced interaction, or indirectly through loop diagram or mixing. Both scenarios are viable and a few categories of models depending on the spin and parity of the mediator are on the market. The natural limitation is to consider only extensions with operators in the Lagrangian with dimension at most four to simplify the picture and to give a separate attention to the infrared physics only.

Depending on the type of the mediator few "portals" to the hidden sector could be identified [14]:

Scalar portal: The most general scenario employing an additional scalar particle is through its interactions with the Standard Model Higgs boson. This includes both operators of third and fourth order resembling the Higgs potential in the Lagrangian

(3)
$$\mathcal{L} \sim \mu S H^+ H + \lambda S^2 H^+ H.$$

Since the best way to look for such type of new particles is through the study of Higgs decay final states and Higgs properties, the most appropriate machines to address this scenario are the high energy colliders.

– Pseudoscalar portal: A possible solution to the strong CP problem is the introduction of a new Peccei-Quinn global U(1) symmetry which is broken spontaneously. The pseudo Nambu-Goldstone boson of this breaking is the axion. The interaction between the axion and the Standard Model fermions is given by the

(4)
$$\mathcal{L} \sim \frac{\partial_{\mu} a}{f_a} \bar{\psi}_f \gamma^{\mu} \gamma_5 \psi_f$$

term in the Lagrangian. While the parameters of the axion, its mass M_a and coupling α_a to the ordinary Standard Model fields are functions of the breaking scale f_a of the Peccei-Quinn symmetry, other axion-like particles (ALPs) may well exist and their parameters are free. The couplings of the ALPs to photons and Standard Model fermions are also arbitrary.

 Neutrino portal: The existing puzzle in the neutrino mass sector provides input for few interesting models explaining this phenomena. The possible existence of a sterile neutrino may lead to the addition of Yukawa term

$$\mathcal{L} \sim Y_N L H N.$$

This sterile neutrino is the Standard Model singlet and could be produced in the early Universe. If the relic abundance and interactions strength with the dark matter are sufficient, they will delay the DM kinetic decoupling and will allow the solution of the problem with the missing-small scale structures like satellite galaxies [15].

– Vector portal:

The most general interaction of an electrically neutral vector particle A' with the Standard Model fermions can be written in the form

(6)
$$\mathcal{L} \sim g' q_f \bar{\psi}_f \gamma^\mu \psi_f A'_\mu,$$

where g' is the universal coupling constant of the new interaction and q_f are the corresponding charges of the interacting fermions.

The extensions of the Standard Model may well involve other new interactions with the matter fermions. They could be made anomaly free (like in the case of B-L as a gauge symmetry) and then the interaction term could be of order $D \leq 4$. The tree level process may again proceed through vector particles that are neutral under any of the Standard Model gauge groups.

In the present review we focus mostly on the vector portal as this is the scenario that is most extensively tested experimentally at low energies. This scenario may include also any of the possible new interactions involving neutral mediators. They all may be grouped in the so-called $dark\ photon\ (DP)$ models. They do not require the introduction of UV physics and can be probed efficiently at high intensity and low energy machines.

2.1. Dark photon models. – We will call dark photon models every model that predicts the existence of a new neutral vector particle (A') which has a non-vanishing coupling to the standard fermions in the form described in eq. (6). This A' could itself be the mediator between the visible and the dark sector but the link can also be realized in different ways.

The origin of the coupling of A' to the fermion fields could arise in various models. Since almost any extension of the Standard Model introduces new symmetries and gauge groups the wide range of possibilities go from maximally universal models to including only single type of fermions or even a single generation. A very subjective list of some of the basic classes, intended to illustrate the rich picture, are presented below.

2.1.1. Kinetic mixing. One of the best motivated dark photon models is the so-called kinetic mixing model, in which a new $U(1)_D$ group is introduced, responsible for the interactions between the particles in the dark sector. It mirrors the hypercharge interactions of the Standard Model particles and its carrier, the dark photon (or the so-called U-boson, dark boson, secluded photon) could mix with the ordinary photon [16-18].

(7)
$$\mathcal{L}_{\text{mix}} = -\frac{\epsilon}{2} F_{\mu\nu} F^{\prime\mu\nu}.$$

When the electroweak symmetry breaks this introduces an effective interaction between the fermions and the dark photon in the form

(8)
$$\mathcal{L} \sim \epsilon e \bar{\psi} \gamma^{\mu} \psi A'_{\mu},$$

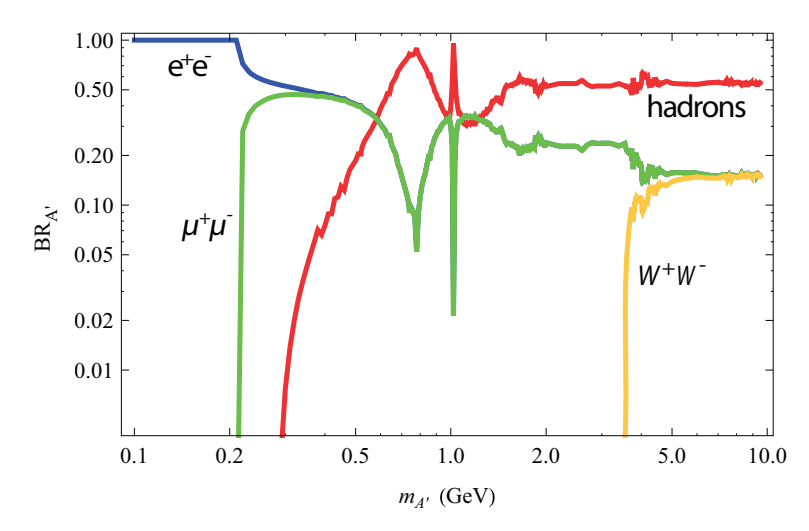


Fig. 1. – Dark photons decay modes and their branching fractions for different dark photon mass values

where the charges of the individual fermions are exactly the electromagnetic ones. The dark photon could be either massive or massless, as in the case of [17]. The latter leads to the appearance of electrically milli-charged particles [19] which are represented by all the particles in the dark sector that couple to A'.

In the described model all the processes are determined by the single parameter, the mixing ϵ . As a result the model benefits from the high predictivity and this is the reason why the kinetic mixing is usually used as a benchmark model describing the phenomenology of the dark photon as a whole. An example for this is the partial decay width of the dark photon, which in the case of $M_{A'} > 2m_l$ and l^+l^- pair in the final state is given by [20]

(9)
$$\Gamma_{A' \to l^+ l^-} = \frac{1}{3} \alpha \epsilon^2 M_{A'} \sqrt{1 - \frac{4m_l^2}{M_{A'}^2}} \left(1 + \frac{2m_l^2}{M_{A'}^2} \right),$$

while for hadrons it can be written as

(10)
$$\Gamma_{A' \to \text{had}} = \frac{1}{3} \alpha \epsilon^2 M_{A'} \sqrt{1 - \frac{4m_{\mu}^2}{M_{A'}^2}} \left(1 + \frac{2m_{\mu}^2}{M_{A'}^2} \right) \times \frac{\Gamma(e^+e^- \to \text{hadrons})}{\Gamma(e^+e^- \to \mu^+\mu^-)} (E = M_{A'}).$$

Summarizing eqs. (9) and (10) the decay fraction of the dark photon into Standard Model particles is shown in fig. 1.

Non-miminal kinetic mixing. The mediator, A', might not be the only accessible state from the dark sector. Since nothing prohibits the dark particles to be light, they can populate an extended mass region down to zero. In its simplest form, the interraction term of a dark fermion, χ , with A' would be similar to QED

(11)
$$\mathcal{L}_{\mathcal{D}} \sim \sqrt{4\pi\alpha_D}\bar{\chi}\gamma^{\mu}\chi A'_{\mu},$$

where α_D is the coupling constant associated with the $U(1)_D$ gauge group in the dark sector.

If $m_{\chi} < 1/2M_{A'}$ the dark photon decay rate to the $\chi\chi$ pair is given by [21]

(12)
$$\Gamma_{A'\to\chi\chi} = \frac{1}{3} \alpha_D M_{A'} \sqrt{1 - \frac{4m_\chi^2}{M_{A'}^2}} \left(1 + \frac{2m_\chi^2}{M_{A'}^2} \right).$$

An interesting possibility appears when $\alpha_D \gg \alpha \epsilon^2$. Such scenario is natural since there is no necessity to suppress the interactions in the hidden sector. Then the dark photon will not decay to visible particles and will escape undetected by most of the present experiments, even if it is produced, since in this case the dominant decay channel would be $A' \to \chi \chi$. However, the dark states could scatter on the matter electrons through the A-A' mixing, with a cross-section given by [22]

(13)
$$\frac{\mathrm{d}\sigma(e\chi \to e\chi)}{\mathrm{d}E_f} = \frac{\alpha_D \epsilon^2}{\alpha} \times \frac{8\pi\alpha^2 m_e (1 - E_f/E)}{(M_{A'}^2 + 2m_e E_f)^2},$$

where E_f is the electron recoil energy. This scenario can also be probed in high intensity primary beam experiments on a target. The low background condition can be provided either through the usage of thick target absorbing the Standard Model interaction products or with a specific detector design.

When $m_{\chi} \gg m_e$ or if there are no light dark matter particles below $m_{A'}$ the dark photon lifetime will be proportional to $1/(\epsilon^2 M_{A'})$.

2.1.2. B-L. Another possibility to connect the dark photon to the Standard Model particles is through gauge group under which the Standard Model fermions are charged. An example of such charge is the (B-L) and the anomaly free gauge group $U(1)_{(B$ - $L)}$. The interaction strength then would be the product of the O(1) charges and a very small coupling constant $g_{(B-L)}$. Then in general there is no limitation to allow for both mechanisms to take place at the same time —kinetic mixing and a direct tree level coupling. By considering mixing with the hypercharge $U(1)_Y$ the most general Lagrangian would be [23]

(14)
$$\mathcal{L} \sim -\frac{1}{4}B_{\mu\nu}B^{\mu\nu} - \frac{1}{4}F'_{\mu\nu}F'^{\mu\nu} + \frac{1}{2}M_{A'}^2A'^2_{\mu} + g_Y j_B^{\mu}B_{\mu} + g_{B-L}j_{B-L}^{\mu}A'_{\mu} + e\epsilon j_{\rm EM}^{\mu}A'_{\mu},$$

where j_B^{μ} and $j_{\rm EM}^{\mu}$ are the hypercharge and the electromagnetic current correspondingly. The additional barion-lepton current

(15)
$$j_{B-L}^{\mu} = (B-L)\bar{f}\gamma^{\mu}f = -\bar{l}\gamma^{\mu}l - \bar{\nu}_{l}\gamma^{\mu}\nu_{l} + \frac{1}{3}\bar{q}\gamma^{\mu}q$$

is responsible for the new type of interactions. In case we want to mix directly with the ordinary photon we have to make the substitution $B^{\mu} \to A^{\mu}$.

The described gauge group includes also interaction of neutrinos with dark photons and can be individually probed through neutrino scattering data. The differential neutrino cross-section as a function of the electron recoil energy T can be written as

(16)
$$\frac{\mathrm{d}\sigma}{\mathrm{d}T}(\nu e^{-} \to \nu e^{-}) = \left[\frac{\mathrm{d}\sigma}{\mathrm{d}T}\right]_{\mathrm{SM}} + \left[\frac{\mathrm{d}\sigma}{\mathrm{d}T}\right]_{\mathrm{DP}} + \left[\frac{\mathrm{d}\sigma}{\mathrm{d}T}\right]_{\mathrm{INT}}.$$

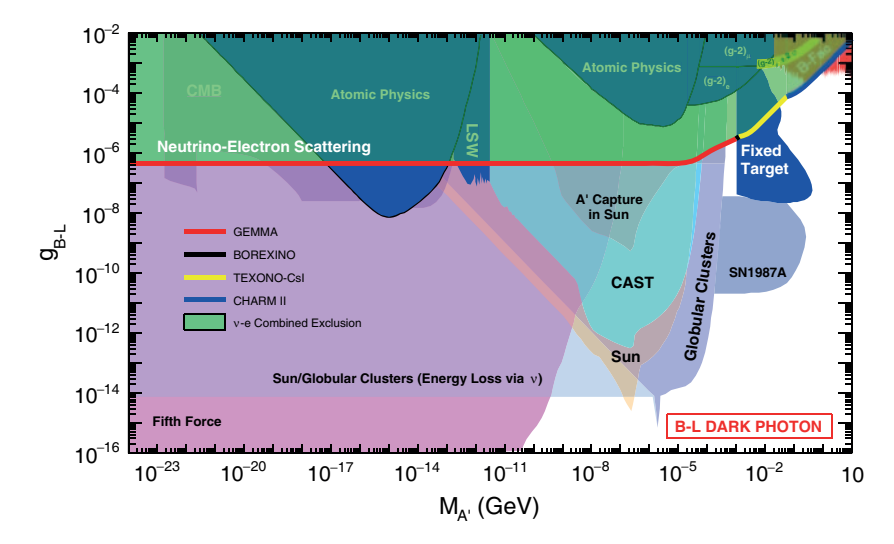


Fig. 2. – Excluded regions in the parameter space g_{B-L} - $M_{A'}$ from neutrino scattering experiments in the case of a new B-L gauge interaction [23].

The Standard Model contribution is suppressed by the Fermi constant G_F

(17)
$$\left[\frac{\mathrm{d}\sigma}{\mathrm{d}T} (\nu e^- \to \nu e^-) \right]_{\mathrm{SM}} = \frac{2G_F m_e}{\pi E_{\nu}^2} (a^2 E_{\nu}^2 + b^2 (E_{\nu} - T)^2 - abm_e T),$$

where the constants a and b depend on the neutrino flavour. The dark photon contribution in the case of light vector mediator is suppressed by the coupling constant g_{B-L}

$$(18) \quad \left[\frac{\mathrm{d}\sigma}{\mathrm{d}T} (\nu e^- \to \nu e^-) \right]_{\mathrm{DP}} = \frac{g_{B^-L}^4 m_e}{4\pi E_{\nu}^2 (M_{A'}^2 + 2m_e T)^2} (2E_{\nu}^2 + T^2 + 2TE_{\nu} + m_e T)$$

and is flavour blind. The proper treatment of the interference term is also crucial for the interpretation of the data to extract the dark photon parameters as shown in [23] and is given by

(19)
$$\left[\frac{\mathrm{d}\sigma}{\mathrm{d}T}(\nu e^{-} \to \nu e^{-})\right]_{\mathrm{INT}} = \frac{g_{B-L}^{2}G_{F}m_{e}}{2\sqrt{2}E_{\nu}^{2}\pi(M_{A'}^{2} + 2mT)} \times f(E_{\nu}, T, m_{e}),$$

where the quadratic function $f(E_{\nu}, T, m_e)$ depends on the neutrino flavour since in the electron neutrino case both the W and the Z boson exchange contribute while in the case of ν_{μ} and ν_{τ} only the Z boson plays a role.

For low masses of the dark photon (O(MeV)) and below) the parameters $m_{A'}$ and g_{B-L} can be significantly constrained from the measurements of the neutrino scattering cross-sections performed by GEMMA [24], BOREXINO [25], TEXONO-CsI [26] and CHARM II [27]. They are consistent with a pure Standard Model contribution and the lack of signal limits the parameter region as shown in fig. 2.

The present data practically excludes the simplest $U(1)_{B-L}$ model with universal coupling as a possible explanation of the $g_{\mu}-2$ anomaly.

 $2^{\circ}1.3$. Leptophilic gauge boson. Apart from models involving interactions of both quarks and leptons to the dark photon, numerous models exist where only one type of fermions is involved. The neutrino scattering data from the previous section indicates that the contribution to the cross-section of the left-handed neutrinos should not exceed G_F . This is satisfied only for small coupling constants [28]. Another possibility are interactions involving only right-handed leptons [29]. The possibility to consider such interactions for muons only allows to explain the present 7σ discrepancy between the measurements of the proton radius [30]

(20)
$$R_p^e = 0.8775(51) \,\text{fm},$$
$$R_p^{\mu} = 0.84087(38) \,\text{fm},$$

performed with electrons and muons. At the same time such a model could also explain the $g_{\mu}-2$. If the dark photon is heavier than the right-handed neutrinos N, an additional decay channel is allowed, $A' \to N\bar{N}$, with a decay width of

(21)
$$\Gamma_{A' \to N\bar{N}} = \frac{1}{6} \frac{g'^2}{4\pi} m_{A'} \left(1 - \frac{m_N^2}{m_{A'}^2} \right) \sqrt{1 - \frac{4m_N^2}{m_{A'}^2}},$$

where g' is the coupling constant of the leptophilic gauge boson.

2.1.4. Flavour non-universal coupling. An example of a model constructed such that the dark sector couples predominantly with a specific flavour is described in [31]. The basic idea is the introduction of a vector-like doublet of fermion fields E and the $SU(2)_D$ group for the dark interactions. The fields

$$(22) E_L^a, E_R^a$$

have the same Standard Model quantum numbers as the right-handed charged leptons. The index a is the $SU(2)_D$ index. The gauge symmetry $SU(2)_D$ is completely broken by the Higgs mechanism through a complex scalar doublet $\langle \phi^a \rangle$. This also induces mixing between E and the Standard Model leptons leading to non-vanishing coupling between the $SU(2)_D$ dark gauge boson multiplet and the ordinary Standard Model leptons. The coupling is suppressed by the small mixing angle which is proportional to the ratio of the vacuum expectation values v_D/v of the ϕ and the Standard Model Higgs, where $v=246\,\mathrm{GeV}$. This assumption is true if the masses of the dark gauge bosons are in the region below 1 GeV. Then the mass mixing is through Yukawa couplings

(23)
$$\mathcal{L} \sim h\bar{\mu}_R \phi_a^* E_L^a + h' \epsilon_{ab} \bar{\mu}_R \phi^{*a} E_L^b,$$

where h and h' are the coupling constants. The chosen type of mixing explicitly breaks the lepton universality and generally one could expect similar terms involving electron and tau-lepton.

This model provides an additional portal to the dark sector —the Higgs one, through the order-four operator $\phi^+\phi H^+H$. However, the measurement of the decay rates of the recently discovered at LHC Higgs boson, which are compatible with the Standard Model, shows that such interaction should be negligible. By construction this model could influence predominantly the muon parameters while leaving the electron ones completely consistent with Standard Model calculations.

- **2**[.]2. Dark photon mass generation. The mass term of the dark photon breaks the gauge invariance of the dark interactions and can be generated through different mechanisms [32].
 - Stückelberg mechanism: The mass term of the gauge vector field A' could be introduced through an interaction term of A' with a scalar of the form

(24)
$$\mathcal{L}_{\text{mass}} \sim \frac{1}{2} (\partial^{\mu} \alpha + m A^{\prime \mu}) (\partial_{\mu} \alpha + m A^{\prime}_{\mu}).$$

In unitary gauge this leads exactly to the well-known mass term for spin-1 field. Such terms in the Lagrangian arise for example in string theories [33] where the Abelian open-string gauge boson couples to a closed-string Ramond-Ramond (RR) axions.

The Stückelberg mechanism could also be viewed as a special case of the Higgs mechanism when the Higgs field mass (or more precisely the vacuum expectation value) goes to infinity. In this case there are no extra particles needed to have massive dark photon and the phenomenology of the processes does not change with respect to the simplest effective model.

- Dark Higgs: A possible mechanism to realize such scenario is through an additional scalar field charged under $U(1)_D$ —"dark Higgs"— which restores the longitudinal polarization of the vector boson. The masses of the dark Higgs and the dark photon arising through spontaneous symmetry breaking of the $U(1)_D$ would be of similar order. Then the additional terms to the "dark" Lagrangian would be

(25)
$$\mathcal{L} \sim \frac{1}{2} m_{A'}^2 A'_{\mu} A'^{\mu} + g' m_{A'} h' A'_{\mu} A'^{\mu} + \frac{1}{2} g'^2 h'^2 A'^2,$$

where h' is the dark Higgs field and g' is the $U(1)_D$ coupling constant. Thus the interactions and the parameters of the dark photon could also be probed through the searches of hidden Higgs fields.

- Interactions of the dark photon with the Standard Model Higgs: In principle it is theoretically possible to include interactions of the Standard Model Higgs with the dark photon. However, as stated above, the present data from LHC largely excludes this possibility.
- 2.3. Dark photon production. While the rates of the possible decays of the dark photon are easy to be predicted, their production rate is not that straightforward in most of the cases. The present review follows the study performed in [34]. Few particular cases could be identified as seen from fig. 3: dark photon production in meson decays, in lepton-on-target experiments, and in proton-on-target experiments:
 - Dark photon production in meson decays: The dark photon can be produced in the decays of the charged and neutral pseudoscalar (P) and vector (V) mesons in the processes $\pi^0 \to \gamma A'$, $V^{\pm} \to \pi^{\pm} A'$, and $P^{\pm} \to \pi^{\pm} A'$. The last process is possible only if the dark photon is massive and the decay rate is proportional to $m_{A'}^2$. The branching fraction of the vector mesons can be extracted from the corresponding

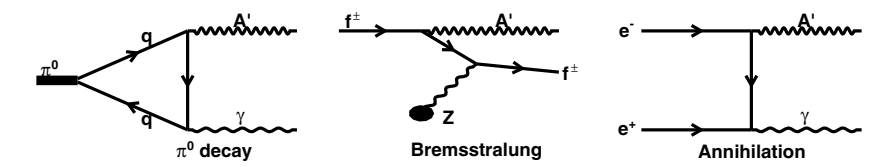


Fig. 3. – Illustration of the different dark photon production mechanisms.

decay mode with a photon in the final state. For example, in the case of vector particle

(26)
$$BR(V^{\pm} \to P^{\pm}A') =$$

$$\epsilon^{2}BR(V^{\pm} \to P^{\pm}\gamma) \frac{(m_{V}^{2} - m_{A'}^{2} - m_{P}^{2})\sqrt{(m_{V}^{2} - m_{A'}^{2} + m_{P}^{2})^{2} - 4m_{V}^{2}m_{P}^{2}}}{(m_{V}^{2} - m_{A'}^{2})^{3}},$$

with a phase space correction depending on the vector meson, pseudoscalar meson, and dark photon masses m_V , m_P , and $m_{A'}$.

– Dark photon production in lepton-on-target processes: A process that is always present in the e-on-target experiments is the bremsstrahlung. In an analogous way A' could be emitted in the so-called A'-strahlung. The production rate could be calculated in the Weizsäcker-Williams approximation [35]. If the electron energy is E_0 and the dark photon is emitted with energy $E_{A'} = xE_0$, then the differential cross-section is

(27)
$$\frac{d\sigma}{dx d \cos \theta_{A'}} \approx \frac{8Z^2 \alpha_{\text{QED}}^3 \epsilon^2 E_0^2 x}{U^2} \frac{\chi}{Z^2} \times \left[(1 - x + x^2/2) - \frac{x(1 - x) m_{A'}^2 E_0^2 x \theta_{A'}^2}{U^2} \right],$$

where $\theta_{A'}$ is the emission angle of A' with respect to the beam electron, Z is the atomic number of the target material,

(28)
$$U = U(x, \theta_{A'}) = E_0^2 x \theta_{A'}^2 + m_{A'}^2 \frac{1-x}{x} + m_e^2 x$$

and for given nuclei

(29)
$$\chi = \chi(E_0, m_{A'}) = \int_{t_{\min}}^{t_{\max}} dt \frac{t - t_{\min}}{t^2} G_2(t),$$

where $t_{\min} = (m_{A'}^2/2E_0)^2$, $t_{\max} = m_{A'}$, and $G_2(t)$ is a general electric form factor [35]. This widely used approximate formula, however, could lead to up to 30% overestimation of the cross-section for low O(1 GeV) beam energies [36].

Another possibility for leptonic production of dark photon is through the annihilation process, with positron beam. In the limit $m_{A'} \to 0$ and $\epsilon = 1$ the cross-section

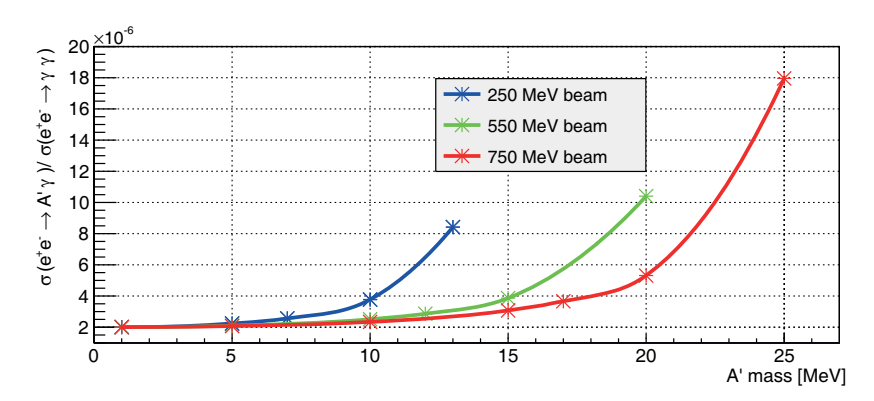


Fig. 4. – Ratio of the cross-sections of the processes $e^+e^- \to \gamma A'$ and $e^+e^- \to \gamma \gamma$ in positron-on-target annihilation, for $\epsilon = 10^{-3}$ and different e^+ beam energies [74].

is two times the ordinary two-photon annihilation

(30)
$$\sigma(e^+e^- \to \gamma A') = 2\epsilon^2 \sigma(e^+e^- \to \gamma \gamma).$$

If $m_{A'}$ cannot be neglected with respect to the center of mass energy \sqrt{s} , the differential cross-section can be obtained, neglecting m_e , from [37]

(31)
$$\frac{\mathrm{d}\sigma(e^+e^- \to \gamma A')}{\mathrm{d}\cos\theta} = \frac{\alpha\epsilon^2}{2s^2(s - m_{A'}^2)} \left(\frac{s^2 + m_{A'}^4}{\sin\theta^2} - \frac{(s - m_{A'}^2)^2}{2}\right)$$

which reduces to (30) for $s \gg m_{A'}^2$ as seen in fig. 4.

For low mass dark photon this process could be an important production mechanism since it allows the reconstruction of the full event kinematics, providing a way to probe long living or invisibly decaying dark photon.

Dark photon production with hadron beams: The differential cross-section for A' production through proton bremsstrahlung has been calculated in the Weizsäcker-Williams approximation [38]. Translating this into differential event rate per proton interaction with nucleus A, the expressions is

(32)
$$\frac{\mathrm{d}N}{\mathrm{d}z\mathrm{d}p_{\perp}^{2}} = \frac{\sigma_{pA}(s')}{\sigma_{pA}(s)}\omega(z, p_{\perp}^{2}),$$

where z is the fraction of the proton momentum carried by A', p_{\perp} is the transverse component of the A' momentum, $s' = 2M(E_p - E_{A'})$ is the reduced centre-of-mass energy after A' emission, and $s = 2ME_p$, and

$$\begin{split} (33) \quad & \omega(z,p_{\perp}^2) = \frac{\epsilon^2 \alpha}{2\pi} \left\{ \frac{1 + (1-z)^2}{z} - 2z(1-z) \left[\frac{2M^2 + m_{A'}^2}{H} - z^2 \frac{2M^4}{H^2} \right] \right. \\ & \left. + 2z(1-z)[1 + (1-z)^2] \frac{M^2 m_{A'}^2}{H^2} + 2z(1-z)^2 \frac{m_{A'}^4}{H^2} \right\} \frac{1}{H} \,, \end{split}$$

where

(34)
$$H(p_{\perp}, z) = p_{\perp}^2 + (1 - z)m_{A'}^2 + z^2 M^2.$$

The hadron cross-section σ_{pA} is dependent on atomic number. Equation (33) is valid under certain conditions, one of which is that the proton is a structureless particle. In high momentum transfer interactions the quark content becomes important and there is also a possibility for quark bremsstrahlung. If a proton form factor is included, the quark contribution is underestimated but such approximation is often used to obtain conservative limits on the dark photon production rate.

3. - Anomalous magnetic moment

The link between the spin \overrightarrow{S} and the magnetic moment \overrightarrow{M} of a particle (gyromagnetic ratio) is given through the parameter g as

$$(35) \overrightarrow{M} = g \frac{q}{2m} \overrightarrow{S},$$

where q and m are the particle charge and mass. The Standard Model predicts a small deviation of g from 2 for the leptons and this anomalous magnetic moment, a = (g-2)/2, can be calculated with extremely high precision by considering QED, weak interactions and hadronic contributions.

(36)
$$a^{\text{SM}} = a^{\text{QED}} + a^{\text{EW}} + a^{\text{hadrons}}$$

If the dark photon exists and interacts with that flavour, it also contributes to the anomalous magnetic moment, at a tree level as shown in fig. 5. The diagram resembles the QED lowest-order contribution. The additional correction for the leptons can be written in the form [39]

(37)
$$a_l^{\rm DP} = \frac{\alpha_{\rm EM} \epsilon^2}{2\pi} * f(m_l, m_{\rm DP}),$$

where $\alpha_{\rm EM}$ is the fine structure constant, $\alpha_{\rm EM}\epsilon^2=\alpha'$ is the interaction strength between the dark photon and the lepton and

(38)
$$f(m_l, m_{\rm DP}) = \int_0^1 \frac{2m_l^2 z(1-z)^2}{m_l^2 (1-z)^2 + m_{\rm DP}^2 z}.$$

The additional factor $f(m_l, m_{\rm DP})$ equals to unity if $m_l \gg m_{\rm DP}$ and $f(m_l, m_{\rm DP}) = 2m_l^2/3m_{\rm DP}^2$ for $m_l \ll m_{\rm DP}$.

Any observed difference between the measured and the predicted value $\Delta a_l = a_l^{\text{theory}} - a_l^{\text{exp}}$ can be interpreted as due to the presence of a dark photon and used to draw limits on its parameters [40]. However one should not forget that in some cases $\epsilon = \epsilon_l$ is flavour dependent and the combination of results obtained with different generation should be done with care.

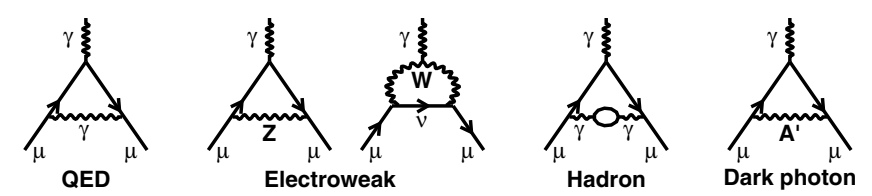


Fig. 5. – Different contributions to the anomalous magnetic moment.

3¹. Dark photons and $(g_e - 2)$. – The value of $(g_e - 2)$ and the electromagnetic coupling constant α are related through the Kinoshita theory [41]

(39)
$$a_e = \frac{g_e - 2}{2}$$

$$= A_1 \frac{\alpha}{\pi} + A_2 \left(\frac{\alpha}{\pi}\right)^2 + A_3 \left(\frac{\alpha}{\pi}\right)^3 + A_4 \left(\frac{\alpha}{\pi}\right)^4 + a \left(\frac{m_e}{m_\mu}, \frac{m_e}{m_\tau}, \text{weak, hadron}\right).$$

The final measurement of a_e performed by the Seattle group [42] using a one-electron quantum cyclotron is with precision almost 15 times better than the previous measurements

(40)
$$a_e = 1159652180.73(0.28) \times 10^{-12}$$
.

This value together with theoretical calculation of the coefficients A_i allows to determine $\alpha_{\rm EM}$

(41)
$$\alpha^{-1} = 137.035999084(51).$$

Any contribution to (g_e-2) different from the ones accounted for in [41] is also absorbed in the value of $\alpha_{\rm EM}$ in eq. (41). In order to decouple the New Physics effects in (g_e-2) the fine structure constant has to be determined in an alternative (and possibly independent) way and compared with the value in (41). Such a result, competitive in precision with the measurement of (g_e-2) , appeared only recently. $\alpha_{\rm EM}$ can be expressed through the Rydberg constant $R_{\infty}=10973731.568508(65)\,\mathrm{m}^{-1}$ [43] as

(42)
$$\alpha_{\rm EM}^2 = \frac{2R_{\infty}h}{cm_e} \,,$$

where m_e is the mass of the electron and h is the Planck constant. From the experimental point of view, more interesting is the introduction of the mass of an arbitrary atom m_a in the expression

(43)
$$\alpha_{\rm EM}^2 = \frac{2R_\infty}{c} \frac{m_a}{m_e} \frac{h}{m_a},$$

since it contains products of measurable ratios $-m_a/m_e$ and h/m_a .

In the case of choosing rubidium, the ratio $h/m_{\rm Rb}$ was deduced from the measurement of the recoil velocity of the Rb atom when it absorbs a photon. An atom interferometry

technique was employed with ultra cold $^{87}{
m Rb}$ absorbing and re-emitting photons from a laser. A single new result

(44)
$$\frac{h}{m_{\rm Rb}} = 4.5913592729(57) \times 10^{-9} \,\mathrm{m}^2 \,\mathrm{s}^{-1}$$

was published in 2011 [44], improving the precision to 1.24×10^{-9} —almost an order of magnitude with respect to the previous measurements.

The ratio $m_{\rm Rb}/m_e$ was extracted from the measurement of the atomic masses of Rubidium and the electron. The ⁸⁷Rb mass was obtained from the ratio $\langle R \rangle$ of the cyclotron frequencies $f=qB/2\pi m$ of two single atoms —a reference and the one under study, simultaneously trapped in a 8.5 Tesla Penning trap [45]. The ratio $\langle R \rangle$ gives the inverse mass ratio. Double ionized ⁸⁶Kr and ⁸⁷Rb ions were used leading to

(45)
$$\langle R \rangle (^{87} \text{Rb}^{2+} / ^{86} \text{Kr}^{2+}) = 0.988510045784(69).$$

By treating the other atomic masses as known references, with uncorrelated uncertainties, preliminary alkali-metal atomic masses were obtained [45], in particular $m(^{87}\text{Rb}) = 86.909180535(10)u$, with precision of 1.2×10^{-10} .

The atomic mass of the electron is derived from measurement of the ratio of the cyclotron frequency $\nu_{\rm cyc}$ of a five times ionized carbon ion and the precession frequency ν_L of the spin of the electron which is bound to that nuclei. This ratio is experimentally clear since both frequencies are sensitive to the local magnetic field which cancels in the ratio. Then the mass of the electron can be expressed as

$$(46) m_e = \frac{g}{2} \frac{e}{q} \frac{\nu_{\text{cyc}}}{\nu_L} m_{\text{ion}},$$

where q is the charge of the ion, e is the electron charge. The bound electron gyromagnetic factor g responsible for the precession frequency is the only external quantity. This factor is significantly different from the free electron g-factor and has to be calculated separately —at tree level it is given by $g_{\text{bound}} = \frac{2}{3} + \frac{4}{3}\sqrt{1 - (Z\alpha)^2}$. Both the measurement of the ratio $\frac{\nu_{\text{cyc}}}{\nu_L}$ and the calculation of the g-factor implicitly assuming the correctness of QED were accomplished by the authors of [46]. The obtained value for the electron mass was

$$(47) m_e = 0.000548579909067(17)u.$$

By combining all the above measurements, each single one of them with precision of a part per billion or better and using the formula in eq. (43), the obtained value for the fine structure constant is

(48)
$$\alpha_{\rm EM}^{-1} = 137.035999037(91)$$

and for the anomalous magnetic moment of the electron is

$$a_e = 0.00115965218073(28).$$

This result is in very good agreement with the one in (40). The difference

(50)
$$a_e(Rb, m_e, m_{Rb}, theory) - a_e(g_e, exp) = (40 \pm 89) \times 10^{-14}$$

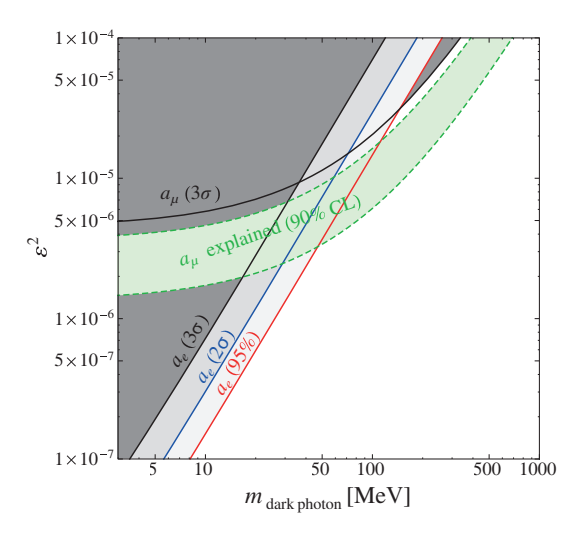


Fig. 6. – Limits on dark photon parameters from the electron and muon anomalous magnetic moment [47].

is consistent with zero New Physics contribution and can be used to set a very strong limit on the dark photon parameters. The excluded region at three sigma level is shown with a straight line in fig. 6.

The described procedure for the determination of α in two different ways can be viewed also as comparison of the $g_e^{\rm free}$ factor of the free electron (used for determination of α through the anomalous magnetic moment) with the $g_e^{\rm bound}$ factor of the bound electron (used to extract α from the measurements with Rb atoms). One may argue that a particular new physics may influence both gyromagnetic ratios and the consistency of the results might still be respected. This might not be easy though since the bound electron g-factor enters in the relation through the parameter $\alpha_{\rm EM}$ that is O(1%), but still possible. So even if the results are impressive with the achieved precision and state-of-the-art calculations more direct data even in the region of the dark photon parameter space that seem excluded by the described analysis is highly desirable.

3[.]2. *Muon anomalous magnetic moment*. – The present theoretical value of the muon anomalous magnetic moment and the experimental value differ by more than three sigma. If the whole discrepancy is attributed to the presence of dark photon the preferred region in the parameter space is shown in fig. 6.

In addition a region in the parameter space can be excluded at three sigma level, also shown in fig. 6.

The observed discrepancy in a_{μ} can be thought of as the first indication of a Lepton Flavour Violating effect. It represents an inconsistency between the electron and the muon data since the determination of $\alpha_{\rm EM}$ from electron data is used in the comparison between the theory and experiment. A good possible check could be a precise measurement of $\alpha_{\rm EM}$ from muonic atoms, however such a result might not be easy to achieve in the near future.



Fig. 7. – Most important experiment working on dark photon searches.

4. - Experimental search for the dark photons

The massive dark photon models are very predictive and the associated phenomenology is therefore very rich. This encouraged a large number of experimental searches exploiting very different techniques together with the study of already collected data sample from the flavour physics experiments of last decade (BABAR, NA48, KLOE). The main effort in searching for the dark photon is at present concentrated in the United States and in particular at the Jefferson Laboratory, see fig. 7, but new initiatives are populating Europe as well. Generally, the biggest uncertainty in the interpretation of the experimental results is related to the existence or the lack of new light states, χ_i , charged under $U(1)_D$. They would open additional dark decay channels changing the exclusions panorama. For this reason exclusion limits have to be carefully interpreted comparing the underlying hypotheses to avoid confusion. In this section we will try to analyse available experimental constraints systematically trying to disentangle the different models. Two major categories of models are identified — "visible" or "invisible"on the basis of the dark photon decay modes which reflect on whether the existence of light dark matter states χ is allowed or not. Visible decay models, even if more popular, are less general because there is no reason a priori to assume that the dark photon is the lightest state in the dark sector.

4.1. Visible decay search techniques. – The experiments devoted to visible decay searches rely on the assumption that the dark photon is the lightest state of the dark sector and therefore may decay only into Standard Model particles. For dark photon mass $M_{A'} < 2m_{\mu}$ the only allowed decay mode is the electron-positron pair. For dark photon mass above the two muon threshold $(M_{A'} > 2m_{\mu})$ the decay into muon pairs is also allowed, while for $(M_{A'} > 2m_{\pi})$ the dark photon can decay into hadrons as well. Regardless of its mass the dark photon always has a significant decay fraction into lepton pairs.

A lot of experimental activity was seen recently. The data mining technique in data samples already collected in the past and the results from dedicated experiments allowed

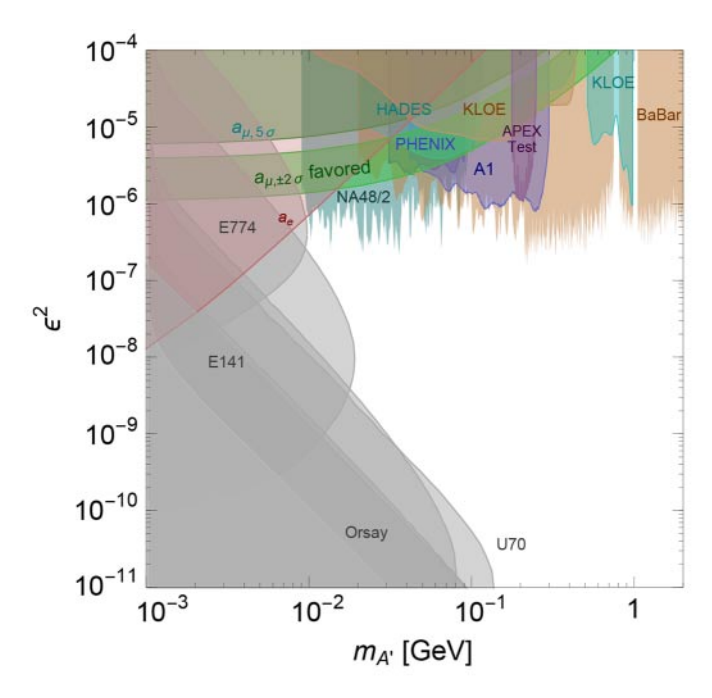


Fig. 8. – Constraints in the ϵ^2 versus $M_{A'}$ plane for dark photons that decay directly to SM particles. (Figure adapted from [85].)

to exclude the $g_{\mu}-2$ favoured parameter region completely in the hypothesis that dark photon decays into Standard Model particles. All the measurements presented in fig. 8 can be classified, according to the applied technique, into three different categories: dump experiments, fixed-target experiments, meson decay experiments.

4.1.1. Dump experiments. In beam dump experiments a high-intensity beam dumped onto a thick fixed target provides the large luminosity needed to probe the weak couplings of the dark photon. Incoming electron or proton beam of energy E_0 scatters on the target and produces dark photons A' with energy $E_{A'}$, usually through A'-strahlung. If the dark photon decays to e^+e^- or $\mu^+\mu^-$ it can be detected behind a sufficiently long shield. All Standard Model particles are absorbed by the combination of a target and a shield allowing only neutral long living and weakly interacting states to survive. Any evidence of a di-lepton decay behind the shield, non-compatible with the expected background, indicates the existence of New Physics particles.

This technique was used in the past to search for different kinds of long-living new particles using very different beams and detectors. Depending on the specific experimental setup with respect to the decay length of the dark photon, the possible physics reach is determined not only by the number of the dumped particles but also by the choice of the beam energy, the length of the shield, and the distance to the detector. Due to different A' production mechanisms and interactions of the primaries with the target and the shield, the dump experiments are classified as electron and proton beam dumps. Electrons beam dump experiments are unable to constrain leptophobic dark photon models, while on the contrary proton beam dump cannot constrain leptophilic models. In this respect the two techniques are complementary and redundant measurements are very important. If a

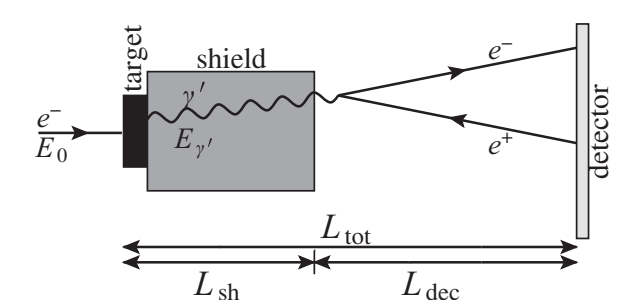


Fig. 9. – Sketch of the setup of an electron beam dump experiment.

particular model allows the dark photon to couple to neutrino (as in the case of $U(1)_{B-L}$ gauge group [49]) its paramaters can be studied from the neutrino-electron scattering data, as described in subsect. 2.1.2.

Electrom beam dump. Several electron beam dump experiments, the properties of which are collected in table I, were operated in the last decades to search for light metastable pseudoscalar or scalar particles. Most of them share a common schematic design, shown in fig. 9, where the thickness of the dump is $L_{\rm sh}$ followed by a decay region with length $L_{\rm dec}$.

KEK

An experiment looking for neutral penetrating particles was conducted in 1986 at the National Laboratory for High Energy Physics (KEK) in Japan [50]. A 2.5 GeV electron linear accelerator injected a total of $27\,\mathrm{mC}$ ($1.69\cdot10^{17}$ electrons) into a tungsten target. In front of a 220 cm long decay volume, an iron dump, lead and plastic was used as shield against the background. The detector system consisted of multi-wire proportional chambers, scintillation counters and a lead glass Cherenkov counter. The experiment did not observe any signal.

Table I. – Summary of electron beam dump experiments reported in [20].

Experiment	Target	E_0 (GeV)	$N_{ m el}$	$L_{\rm sh}~({ m m})$	$L_{\rm dec}$ (m)
KEK [50]	W	2.5	$1.69 \cdot 10^{17}$	2.4	2.2
E141 [51]	W	9	$2 \cdot 10^{15}$	0.12	35
E137 [52]	Al	20	$1.87\cdot10^{20}$	179	204
E774 [53]	W	275	$5.2 \cdot 10^{9}$	0.3	2
Orsay [54]	W	1.6	$2. \cdot 10^{16}$	1	2

E141 at SLAC

A search for short lived axions was performed at SLAC in 1987 [51]. The experiment used an electron beam of $E_0 = 9 \,\mathrm{GeV}$ dumped onto a 12 cm tungsten target, for a total of $2 \cdot 10^{15}$ electrons (0.32 mC). Following an evacuated beam pipe, a spectrometer was placed 35 m downstream of the dump to look for positrons with energy in the range between 70% and 90% of E_0 . A large part of the beam pipe was surrounded by lead and concrete shielding to reduce the background. In the last 5 m the pipe had a diameter of 7.5 cm defining the angular acceptance of 1.1 mrad. From the background-subtracted number of positrons observed at different energies the authors of [20] obtained a 95% C.L. upper limit, assuming a Gaussian signal, on the basis of 3419 background events.

E137 at SLAC

Another experiment to look for neutral metastable penetrating particles was carried out at SLAC in 1988 [52] with a 20 GeV electron beam dumped onto an aluminium target. A 179 m thick hill served as dust shielding and was followed by a 204 m wide open valley as decay region. The experiment dumped a total of $1.86 \cdot 10^{20}$ electrons in two phases, the first one consisting of 9.5 Coulomb and the second one of 20.4 Coulomb. The detector was an electromagnetic shower counter perpendicular to the beam axis with dimensions $2 \text{ m} \times 3 \text{ m}$ in the first and $3 \text{ m} \times 3 \text{ m}$ in the second phase. The experiment reported that no candidates for axion-like events with deposited energy above 3 GeV were observed.

E774 at Fermilab

In 1991, a 275 GeV electron beam at Fermilab was used to search for short-lived neutral bosons decaying to e^+e^- [53]. A 30 cm long tungsten electromagnetic calorimeter was used as target. A total of $5.2 \cdot 10^9$ electrons were dumped onto it. Behind the shield a 2 m long decay region was followed by four scintillation counters. A second electromagnetic calorimeter, placed 7.25 m downstream of the dump, was used to trigger the data acquisition. No candidate e^+e^- pairs were found.

Orsav

In 1989 a total of $2 \cdot 10^{16}$ electrons with an energy of 1.6 GeV provided by the Orsay linac were dumped onto a tungsten target in a search for light Higgs bosons [54]. The dump had a total length of 1 m and was surrounded by lead shielding. Behind a 2 m long and 10 cm wide decay volume inside a concrete wall, a combination of scintillation and lead-glass Cherenkov counters was used to detect either electrons or positrons with energy larger than 0.75 GeV. No evidence of signal was reported.

The lack of New Physics signal in these experiments was reinterpreted in term of dark photon constraint in [35] and recently in [20]. Exclusions presented in [20] were obtained in the kinetic mixing approach and are summarized in fig. 10. The MadGraph [55] simulation code was used to describe the different experimental condition in table I. Monte Carlo simulation of the A' production through A'-strahlung followed by its decay into e^+e^- was obtained. A geometrical acceptance, specific for each of the experimental setups, was determined by studying the angular distribution of A' decay products. However, the excluded regions in fig. 10 may be easily evaded by models with non-universal dark photon couplings to fermions (for example the leptophobic $U(1)_B$).

Proton beam dump. The description of the dark photon production in proton-on-target collisions is a complicated process. So far, there are no universally accepted calculation

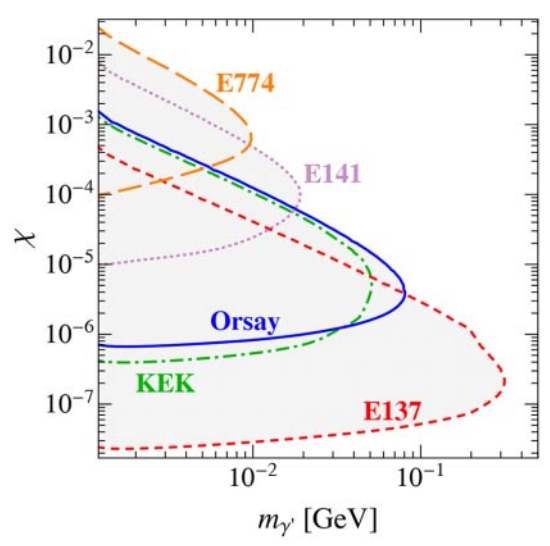


Fig. 10. – Limits on the dark photon mass $m_{A'}$ and kinetic mixing χ from different electron beam dump experiments [20].

tools available for the computation of production rates and distributions of beyond-the-Standard-Model vector particles. In proton dump experiments dark photon can be produced either directly, via proton or lepton A'-strahlung, or indirectly —in mesons decay chains like $\pi^0 \to \gamma A'$. The leptons and mesons are secondary particles produced either by proton scattering off the target or in the electromagnetic and the hadronic showers developed in the dump material. A summary of the most relevant for this review proton beam dump experiments and their properties is reported in table II.

Table II. - Summary of proton beam dump experiments.

Experiment	Target	E_0 (GeV)	N_p	$L_{\rm sh}~({ m m})$	$L_{\rm dec}$ (m)
CHARM [56]	Cu	400	$2.4 \cdot 10^{18}$	480	35
PS191 [57]	Be	20	$8.6\cdot10^{18}$	128	12
NOMAD	Be	450	$4.1\cdot 10^{19}$	835	7.5
NuCal [38]	Al	70	$1.7\cdot 10^{18}$	64	23

CHARM

The CHARM experiment used a 400 GeV proton beam from CERN SpS with a total number of $2.4 \cdot 10^{18}$ protons impinging on a copper target. CHARM searched for decays $\nu_h \to \nu e^+ e^-$ of heavy neutrinos in the ν_h mass range from 10 MeV to 1.8 GeV, with ν_h produced in the decays of π , K and D mesons. The CHARM decay detector (DD), located at the distance of 480 m from the target, consisted of decay volume of $3 \times 3 \times 35$ m³, three chamber modules located inside the decay volume to detect charged tracks, followed by a calorimeter. The occurrence of $A' \to e^+ e^-$ decays would appear as an excess of $e^+ e^-$ pairs in the CHARM detector above those expected from standard neutrino interactions. No excess was observed in the collected data sample. The lack of beyond-the-Standard-Model signal in the CHARM experiment was interpreted in terms of vector portal in [58].

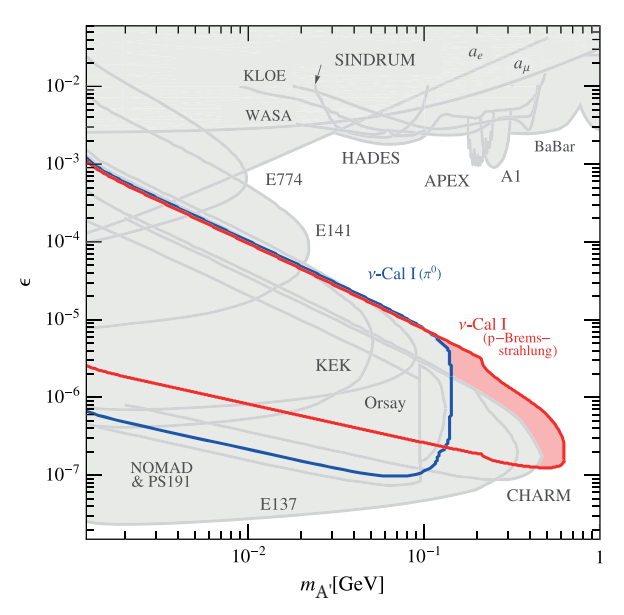


Fig. 11. – Limits on the dark photon mass $m_{A'}$ and kinetic mixing χ from different proton beam dump experiments [38].

PS191

The PS191 beam dump experiment was performed at PS, CERN during the '80s to search for decay products of heavy neutrino ν_h [57]. The investigated decay channels were $\nu_h \to e^\pm \pi^\mp$ and $\nu_h \to e^+ e^- \nu$. A 19.2 GeV proton beam from CERN Proton Synchrotron interacted in a beryllium target (80 cm length). Behind the target there was a 49.1 m long tunnel where the charged secondary pions and kaons were free to decay. Finally, a $\sim 65\,\mathrm{m}$ dust shield followed. It was able to absorb meson decay products and the beam remnants. The detector was located in a pit whose centre was 128 m away from the target and 40 mrad off the beam axis. It consisted of two parts: a 12 m long volume of $18\,\mathrm{m}^2$ cross-section area where neutrinos decay products were detected by chambers with low material content, and an electromagnetic calorimeter of ~ 7 radiation lengths in which showers from electrons and photons were detected.

ν -Cal

The ν -Cal experiment took data from a beam dump at the U70 accelerator, where $1.71 \cdot 10^{18}$, 70 GeV protons were delivered to an iron target during a three months exposure in 1989. Searches for axions and light Higgs bosons were reinterpreted in terms of hidden vectors decaying to leptons in [38], where dark photon production in both π^0 decays and proton bremsstrahlung were considered (see fig. 11).

NOMAD

The NOMAD was a short base-line experiment aimed to search for $\nu_{\mu} \to \nu_{\tau}$ oscillations using CERN SpS neutrino beam. No evidence for oscillations was found. Recent reinterpretation of this result in terms of the dark photon models led to the exclusions in fig. 11.

The exclusion limits obtained with proton beam dump experiments largely overlap with regions already excluded by the electron beam dump ones. Nevertheless the different

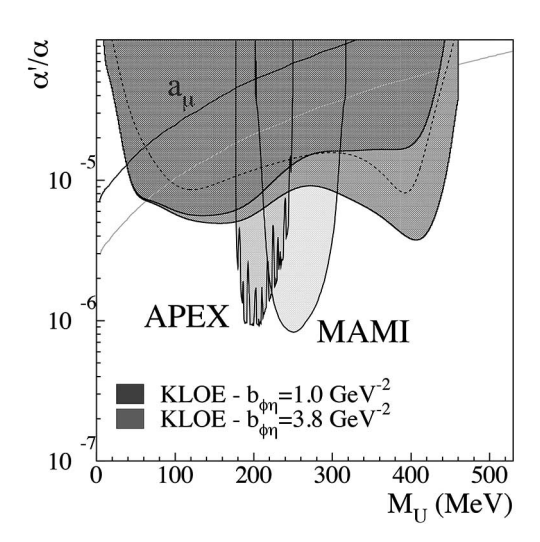


Fig. 12. – KLOE limit for the process $\phi \to \eta A' A' \to e^+e^-$ [60].

production mechanism strongly motivates these measurements as well. One should note that in case of a dark photon model with a non-universal coupling to the SM fermions, as described in sect. 2.1, the exclusions from proton machines are not valid for leptophilic dark photon and the ones from the electron machines —not valid for the leptophobic case.

4.1.2. Meson decay experiments. In the kinetic mixing scenario the dark photon can be produced in the decays of most of the mesons, whenever photons are produced. For this reason it is easy to constrain the dark photon parameter space by using the huge data samples accumulated by the flavour factories (BaBar, KLOE, NA48). Several results from meson decays populate the region of $\epsilon > 10^{-4}$ in a wide mass range in fig. 8. The region below 10^{-4} is difficult to access with this technique because of the lack of statistics and the increased dark photon lifetime.

4.1.3. Searches for dark photon at KLOE. The KLOE detector operates at the INFN Laboratori Nazionali di Frascati ϕ -factory DA Φ NE, an e^+e^- collider running at ϕ -meson mass centre-of-mass energy, $m_{\phi} \sim 1.019 \, \text{GeV}$. The KLOE collaboration has been very active in the dark photon searches since the 2012. In the early period the possibility of dark photon production in the ϕ -meson decay was explored. The collaboration published two searches for the process $\phi \to \eta A' A' \to e^+ e^-$ using two different η tagging technique. In the early paper [59] the η was tagged only by the $\eta \to \pi^+\pi^-\pi^0$ decay while in [60] the $\eta \to \pi^0 \pi^0 \pi^0$ decay was added. The new search was performed on a data sample of 1.7 fb⁻¹, corresponding to approximately 6.10^9 produced ϕ mesons. The search was performed through a bump hunt technique on the $m_{e^+e^-}$ spectrum using a smoothing function to describe the $\phi \to \eta e^+ e^-$ background. The invariant-mass resolution is \sim 2 MeV for $m_{A'} < 350 \text{ MeV}$, improving to 1 MeV for higher values. The analysis assumed that the A' decays only to lepton pairs, with universal coupling to electrons and muons. The extraction of the limit on the α/α' parameter was related to the parametrization of the transition form factor for the process $\phi \to \eta \gamma^*$ as well. Figure 12 shows the exclusion limits for two different values of the form factor slope $b_{\phi\eta}$. The two resulting curves

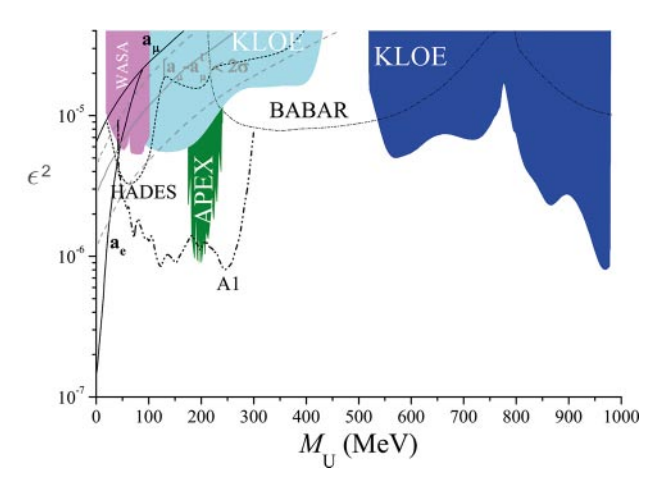


Fig. 13. – KLOE exclusion limit for $e^+e^- \to A'\gamma A' \to \mu^+\mu^-$.

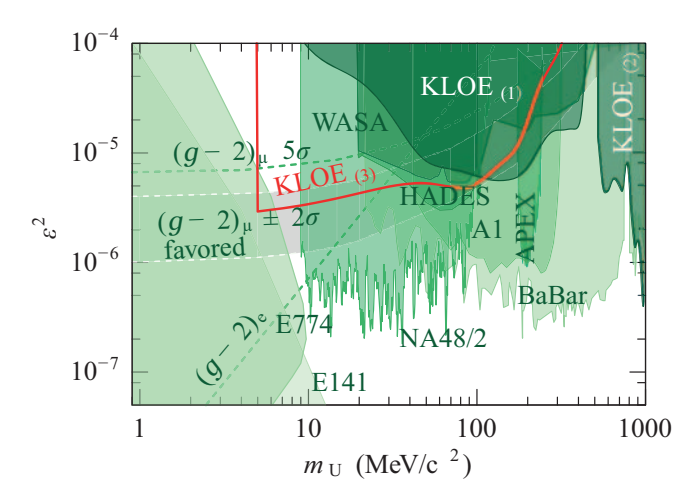


Fig. 14. – KLOE exclusion limits on the dark photon parameters (shown with red curve) from the channel $e^+e^- \to A'\gamma$, $A' \to e^+e^-$ [62].

overlap at low m_{ee} values, while the limit obtained using $b_{\phi\eta}=3.8$ gives an increasingly larger exclusion region up to $\sim 400\,\mathrm{MeV}$. In 2013 KLOE published a second search using the data collected in 2002 with an integrated luminosity of 239.3 pb⁻¹. The search was aimed to identify the process $e^+e^- \to A'\gamma$, $A' \to \mu^+\mu^-$. The KLOE collaboration searched for a peak in the di-muon mass spectrum. The dominant background process was $e^+e^- \to \mu^+\mu^-(\gamma)$ [61] where the photon appeared as an initial-state radiation from e^+ or e^- . The signal window for the bump searches took into account the $m_{\mu\mu}$ resolution which varies from 1.5 MeV to 1.8 MeV, as the mass increases. The resulting exclusion plot on the kinetic mixing parameter ϵ^2 , in the 520–980 MeV mass range, is shown in fig. 13. The sensitivity loss due to the ρ meson around 770 MeV is a result of the suppression of the decay $A' \to \mu^+\mu^-$ due to the increasing fraction of hadronic decay modes (see fig. 1).

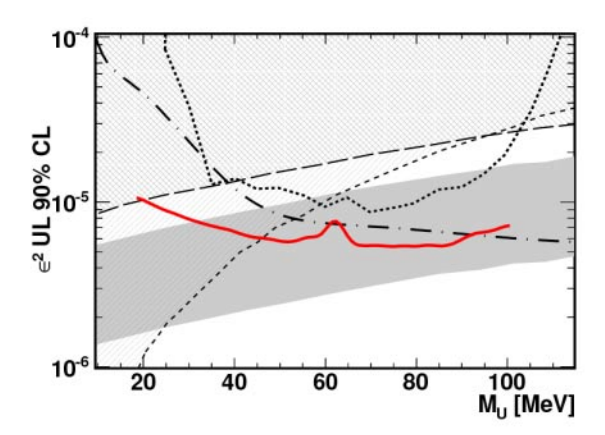


Fig. 15. – WASA limit for the process $\pi^0 \to \gamma A' A' \to e^+ e^-$ [63].

Recently, a new result was released by the KLOE collaboration studying $e^+e^- \to A'\gamma$, with A' decaying into e^+e^- pair [62]. The reach is complementary to the previous analysis because the sensitivity is expected to increase as $m_{A'}$ approaches $2m_e$ due to the dramatic increase in the expected cross-section. The 3 final-state particles of this process were the same as the dominant background represented by the Bhabha scattering. The distinct feature of the dark photon process is a Breit-Wigner resonant production peak (at the A' boson mass) in the invariant-mass distribution of the e^+e^- pair. To reduce the centre-of-mass energy of the fixed-energy collider, and thus scan the range of possible A' masses down to $2m_e$, KLOE used initial-state radiation (ISR). With 1.54 fb⁻¹ of KLOE data collected during 2004-2005, no signal peak was observed, leading to the exclusion shown in fig. 14.

4.1.4. WASA at COsy. The dark photon search in π^0 decays published by the WASA experiment [63] was based on data collected during one-week WASA-at-COSY run carried out in 2010. The π^0 mesons were produced in proton-proton interactions at a kinetic beam energy of 550 MeV, which was 3 MeV below the two pion production threshold. The data sample collected contained $1.8 \cdot 10^6$ reconstructed $\pi^0 \to e^+e^-\gamma$ decays, with a small contamination of $\pi^0 \to \gamma\gamma$ with a photon conversion. The upper limits for the A' boson branching ratios as a function of $m_{A'}$ were obtained by comparing the expected and the observed number of events in each mass bin, in the mass range 20 MeV $< m_{A'} < 100$ MeV. The upper limits for the ϵ^2 parameter was obtained from the branching ratio with the formula

(51)
$$\frac{\Gamma(\pi^0 \to \gamma A')}{\Gamma(\pi^0 \to \gamma \gamma)} = 2\epsilon^2 |F(M_{A'}^2)|^2 \left(1 - \frac{M_{A'}^2}{M^2}\right)^3.$$

The resulting upper limits in the e^2 versus mass diagram are shown in fig. 15.

4.1.5. HADES at GSI. The High-Acceptance DiElectron Spectrometer, HADES, experiment operates at the GSI Helmholtzzentrum für Schwerionenforschung in Darmstadt, where it uses the beam from the heavy-ion synchrotron SIS18 in the few GeV beam energy range. HADES published the results of a search for a $A' \rightarrow e^+e^-$ decay signal

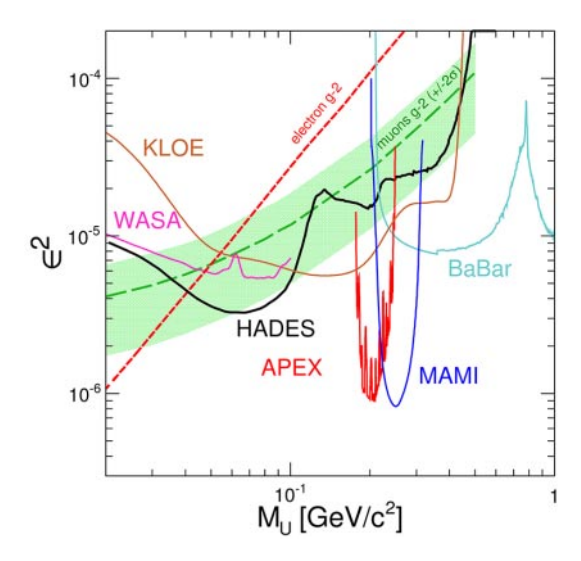


Fig. 16. – HADES exclusion limit for $A' \to e^+e^-$ extracted from light mesons decays [64].

in inclusive dielectron spectra obtained from $3.5\,\mathrm{GeV}$ [64] proton-induced reactions on either a liquid-hydrogen target or a solid niobium target, as well as $\mathrm{Ar}(1.756\,\mathrm{GeV/u}) + \mathrm{KCl}$ reaction. The reconstructed e^+e^- invariant-mass distribution consisted of a superposition of contributions from different sources, which at masses below $0.6\,\mathrm{GeV/c^2}$ were mainly the electromagnetic decays of the π^0 , the η , and the Δ resonance. The search for a narrow resonant state in the e^+e^- mass distributions was conducted by fitting the measured spectra with the sum of a 5th order polynomial and a Gauss peak of fixed position $m_{A'}$ and fixed σ obtained from MC simulation at each different mass.

The excluded region by HADES experiment is shown in fig. 16.

41.6. Searches for dark photon at BaBar. The BaBar collaboration recently published a comprehensive search for dark photons in the reaction $e^+e^- \to A'\gamma$, $A' \to \ell^+\ell^-$ ($\ell = e, \mu$) using 514 fb⁻¹ of data collected mostly at the $\Upsilon(4S)$ resonance, but also at the $\Upsilon(3S)$ and $\Upsilon(2S)$ peaks, and in the vicinity of these resonances as well [65]. The signal yield as a function of $m_{A'}$ was extracted by performing a series of independent fits to the dielectron and the reduced dimuon mass spectra for each beam energy. The fits were performed in the range $0.02 < m_{A'} < 10.2 \,\text{GeV}$ (0.212 $< m_{A'} < 10.2 \,\text{GeV}$) for the dielectron (dimuon) sample. For the purposes of determining the mass steps, the signal resolution was estimated by Gaussian fits to several simulated A' samples, and interpolated to all other masses. It varied between 1.5 and 8 MeV over the whole accessible mass range. A total of 5704 (5370) mass hypotheses for the dielectron (dimuon) channel were tested. No significant signal was observed by the BaBar collaboration and upper limits on the mixing strength ϵ at the level of 10^{-4} – 10^{-3} were set. In fig. 17 the exclusion limit by BaBar is shown. These results also supersede and extend the constraints based on a search for a light CP-odd Higgs boson performed at BaBar with a smaller data set [66]. This search sets the strongest constraint on dark photon decaying into visible particles in a very large region on the parameter space, up to 10 GeV, leaving only the region below $m_{A'} < 30 \,\mathrm{MeV}$ as a possible solution to the $(g_{\mu} - 2)$ anomaly.

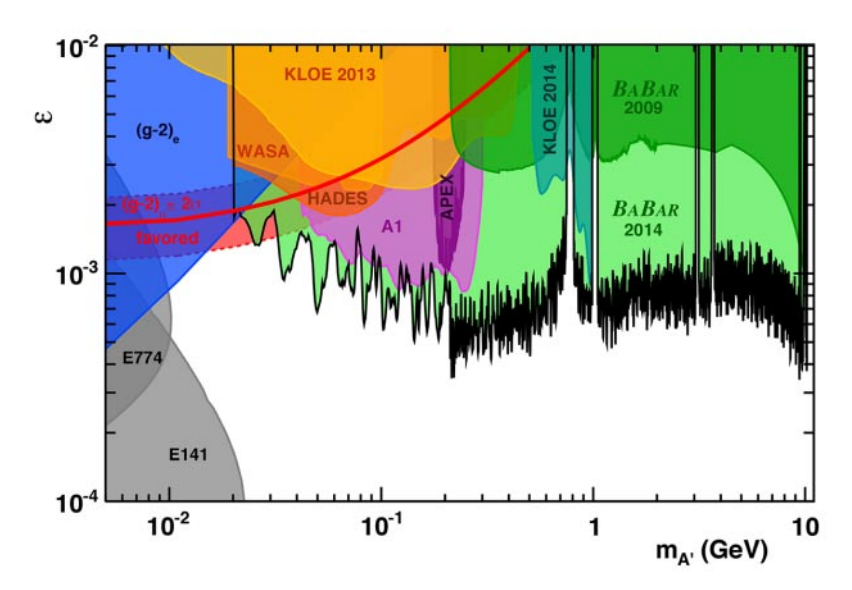


Fig. 17. – BaBar preliminary exclusion limits on the channel $e^+e^- \to A'\gamma$, $A' \to \ell^+\ell^-$ [65].

4.1.7. Dark photon in π^0 decays by NA48/2. High intensity kaon experiments, just like the proton dump, are suitable for searches for dark photons in the π^0 decay as well. NA48/2 at CERN, which took data in 2003-2004, was exposed to $\sim 2 \cdot 10^{11}~K^{\pm}$ decays leading to a sample of $1.69 \cdot 10^7$ fully reconstructed $\pi^0 \to \gamma e^+ e^-$ decays. NA48/2 looked for a dark photon in the decay chain $\pi^0 \to A'\gamma$, $A' \to e^+ e^-$ assuming that A' decays only into SM fermions (BR($A' \to e^+ e^-$) = 1). The expected branching fraction of the $\pi^0 \to A'\gamma$ decay is [22]

(52)
$$\mathrm{BR}(\pi^0 \to \gamma A') = 2\epsilon^2 \left(1 - \frac{m_{A'}^2}{m_{\pi^0}^2}\right)^3 \mathrm{BR}(\pi^0 \to \gamma \gamma).$$

The analysis was performed assuming prompt dark photon decay, therefore the dark photon production and decay signature are identical to that of the Dalitz decay $\pi_D^0 \to \gamma e^+ e^-$ which represented an irreducible background and reduced the sensitivity. The NA48/2 experiment provided pure π_D^0 samples by selecting $K^\pm \to \pi^\pm \pi^0$ and $K^\pm \to \pi^0 \mu^\pm \nu$ ($K_{2\pi}$ and $K_{\mu 3}$) decays. A scan for a dark photon signal in the mass range $9\,\mathrm{MeV}/c^2 \le m_{A'} < 120\,\mathrm{MeV}/c^2$ was performed. No dark photon signal was observed, providing new and more stringent upper limits on the mixing parameter ϵ^2 in the mass range $9-70\,\mathrm{MeV}/c^2$. The obtained upper limits at 90% C.L. [67] on the mixing parameter ϵ are displayed in fig. 18. In combination with other experimental searches, this result ruled out the dark photon as an explanation for the muon $(g_\mu - 2)$ anomaly under the assumption that the dark photon couples to quarks and decays predominantly to SM fermions.

4.1.8. Dark photon searches in heavy ion collisions. Heavy ion collisions are a good source of π^0 , η , and ω mesons due to the large particle multiplicity produced in each single collision. Large amount of photons and therefore dark photons can potentially be produced by these mesons decays. Searches for the dark photon were recently published by both Phoenix and ALICE collaborations. The PHENIX experiment at the BNL

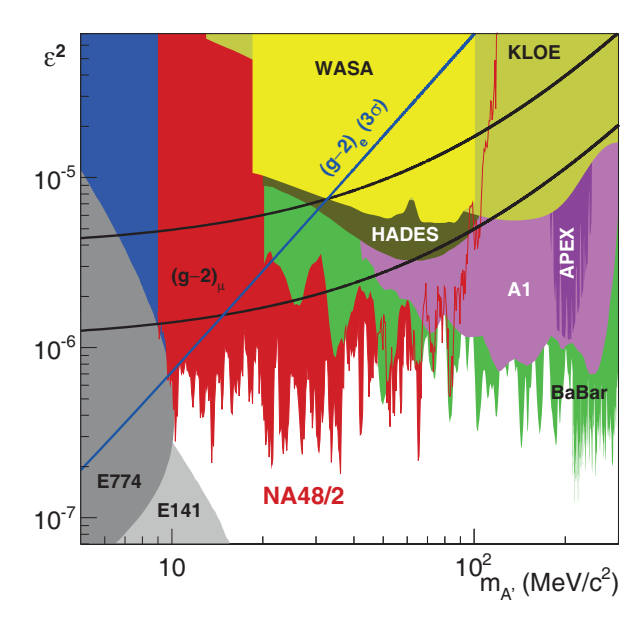


Fig. 18. – Upper limits obtained by NA48/2 at 90% C.L. on the mixing parameter ϵ^2 versus the dark photon mass $m_{A'}$, compared to other published exclusion. Figure taken from NA48/2 COLLABORATION (BATLEY J. R. et al.), Phys. Lett. B, **746** (2015) 178 http://dx.doi.org/10.1016/j.physletb.2015.04.068

Relativistic Heavy Ion Collider searched for a dark photon in $\pi^0 \to \gamma e^+ e^-$ and $\eta \to \gamma e^+ e^-$ decays by combining data samples of 2006, 2008 and 2009 data taking periods. An upper limit of $\sim 2\cdot 10^{-6}$ on ϵ^2 at 90% C.L. was obtained, for the mass range 30 MeV/ $c^2 < m_{A'} < 90 \, \text{MeV}/c^2$ [68]. The ALICE collaboration at the Large Hadron Collider also searched for A' by analysing the data collected during RUN1 and looking for $e^+ e^-$ pairs. A preliminary result was released recently, with a limited statistical sensitivity similar to that of Phoenix. Unfortunately these exclusions fall in a region already strongly constrained by NA48/2 limit [67]. Both ALICE and PHENIX experiments are planning to collect more data in the near future and can possibly improve their results.

4'2. Fixed-target experiments. – Fixed-target experiments using high-current electron beams are an excellent place to search for A''s with masses in the GeV range. Already existing spectrometers were used at JLab and MAMI to search for resonance in the invariant-mass spectrum of e^+e^- pairs produced by electron-on-target collisions. Test runs on the APEX at JLab and A1 at MAMI are examples of early dedicated efforts to constrain the dark photon parameter space. The physical process investigated is the scattering of an electron beam on a fixed target which induces the bremsstrahlung emission of a dark photon, subsequently decaying into a pair of SM leptons. The decay particles are detected and their invariant mass reconstructed, which allows to search for a bump in the invariant-mass spectrum caused by the hidden gauge boson. The A' will manifest itself by a very sharp peak, while the radiative background resulting from the corresponding QED process is described by a smooth distribution.

4.2.1. APEX test run. The A Prime EXperiment (APEX) is a double-arm spectrometer that took data at Jefferson Laboratory hall A in July 2010. An electron beam (left-to-right in fig. 19) was incident on a thin tantalum foil target. Two septum magnets of

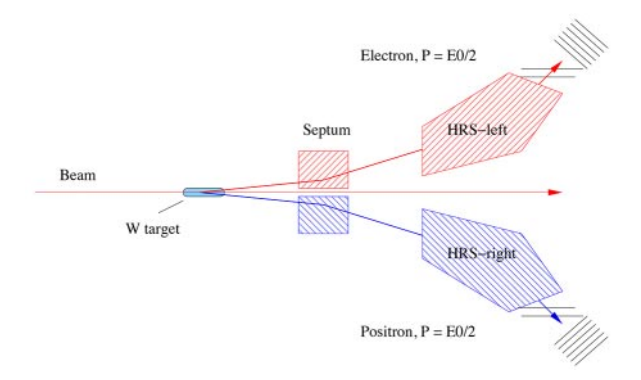


Fig. 19. – Layout of the APEX experiment.

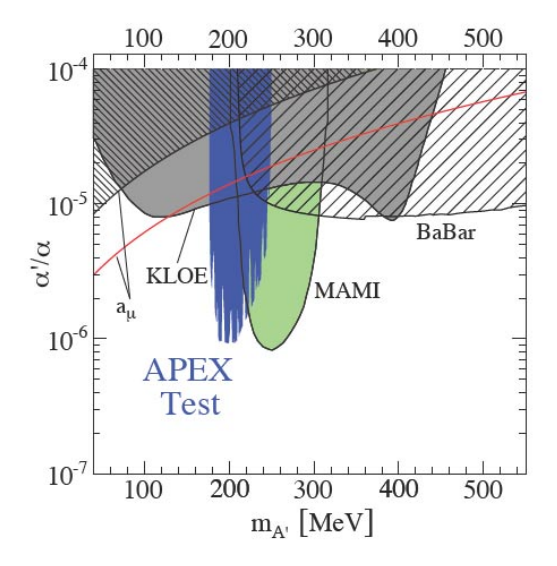


Fig. 20. – APEX test run exclusion limit [69].

opposite polarity deflected the charged particles to larger angles into two vertical-bend high resolution spectrometers. They were adjusted to select electrons and positrons carrying close to half of the incoming beam energy. The spectrometer contained a set of detectors to accurately measure momentum, direction, and identity of the particles as well. The APEX sensitivity to A' depends critically on precise reconstruction of the invariant mass of e^+e^- pairs. Due to the excellent relative momentum resolution $O(10^{-4})$ of the spectrometers, the mass resolution was dominated by the angular resolution.

The test run used a $(2.260\pm0.002)\,\mathrm{GeV}$ electron beam with an intensity up to $150\,\mu\mathrm{A}$ incident on a tantalum foil of thickness $22\,\mathrm{mg/cm^2}$. A bump search was performed on the invariant e^+e^- mass using a binned profile likelihood ratio with $0.05\,\mathrm{MeV}$ bins. The APEX test run data showed no significant signal of $A' \to e^+e^-$ in the mass range 175–250 MeV establishing an upper limit of $\epsilon^2 \sim 10^{-6}$ at 90% confidence level [69] as shown in fig. 20. The full experiment plans to run at several beam energies, to have enhanced mass coverage from a 50 cm long multi-foil target, and to acquire ~ 200 times more data.

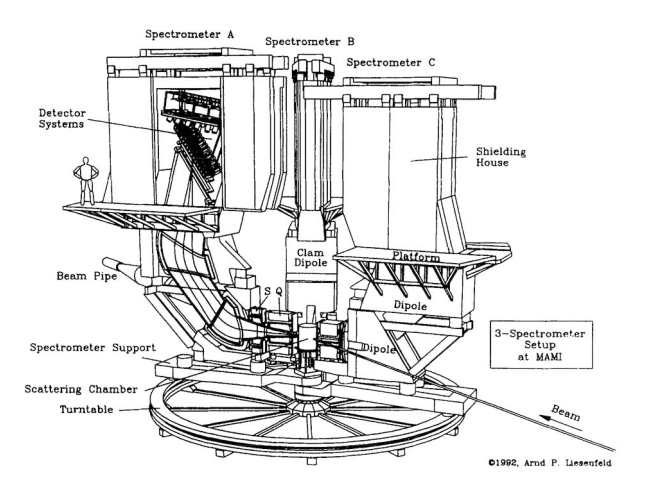


Fig. 21. – Layout of the MAMI 3 spectrometers.

4.2.2. A1 experiment at MAMI. The A1 experiment performed a dark photon search using the A1 Collaboration spectrometer setup at the Mainz Microtron. An unpolarized electron beam with a beam energy ranging from 180 to 855 MeV and a beam current of $80\,\mu\text{A}$ was incident onto an optimized target made of different assembly of tantalum foils. For the detection of the lepton pair from the decay of a possible dark photon, the spectrometers A and B of the A1 setup (fig. 21) were placed at their minimal angle. The two spectrometers were equipped with four layers of vertical drift chambers for position resolution, two layers of scintillator detectors for trigger and timing purposes, and gas Cherenkov detectors for pion-electron separation and further background reduction. For the identified lepton pairs, the invariant pair mass was determined by the four-momenta of the leptons resulting in a resolution which varied between $210 \,\mathrm{KeV}/c^2$ in the lowest mass range up to $920 \,\mathrm{KeV}/c^2$ for the highest beam energy setting. The estimated peak shape was used to define the mass ranges in which the exclusion limits were determined using the Feldman-Cousins algorithm. No significant signal for a dark photon was detected [70] which translated into 2σ limits in terms of the ϵ mixing parameter, as shown in fig. 22. The exclusion limit in the region of the $(g_{\mu}-2)$ anomaly of the muon was improved considerably over a large dark photon mass range.

4'3. Invisible decay search techniques. – The invisible decay searches are based on the hypothesis that at least one new dark sector particle χ of mass lower than $m_{A'}/2$ exists in the dark sector. Under this rather general assumption the dark photon predominantly decays to non-SM states, escaping detection in the past experiments. All branching ratios of the A' decays into Standard Model particles are therefore suppressed by a factor ϵ^2 , strongly reducing the effectiveness of the visible decay searches. As a result, the parameter space for invisible decays is much less constrained by direct searches as shown in figs. 23 and 24. There are several experimental strategies proposed so far to detect the dark photon in this scenario. The first one consists of detecting the dark matter particles χ obtained in the decay of dark photon produced by A'-strahlung into a dump, by means of their scattering in a massive downstream detector. The second technique consists in searching for missing mass into kinematically constrained processes regardless of the A' decay chain. Being described by different models involving different

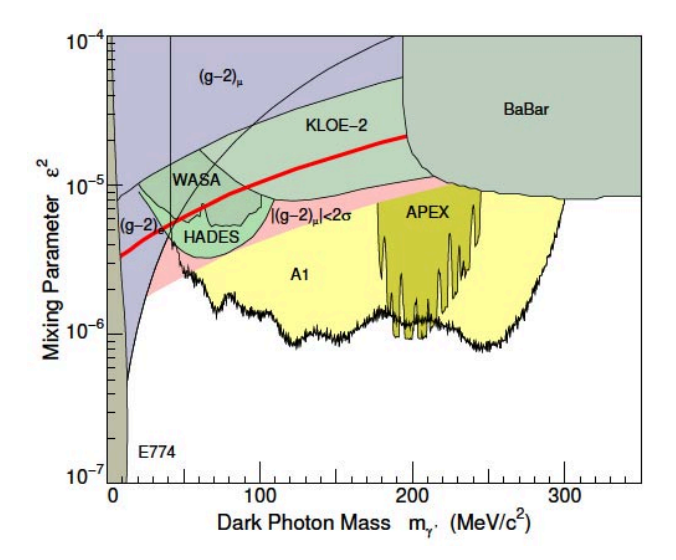


Fig. 22. – A1 experiment exclusion limit [70].

numbers of free parameters, the exclusions obtained with the two different techniques can not be directly compared. For this reason they are represented in two different diagrams in fig. 23 and fig. 24. Indirect limits coming from $(g_{\mu}-2)$, $(g_{e}-2)$, and kaon decays are common to the two scenarios.

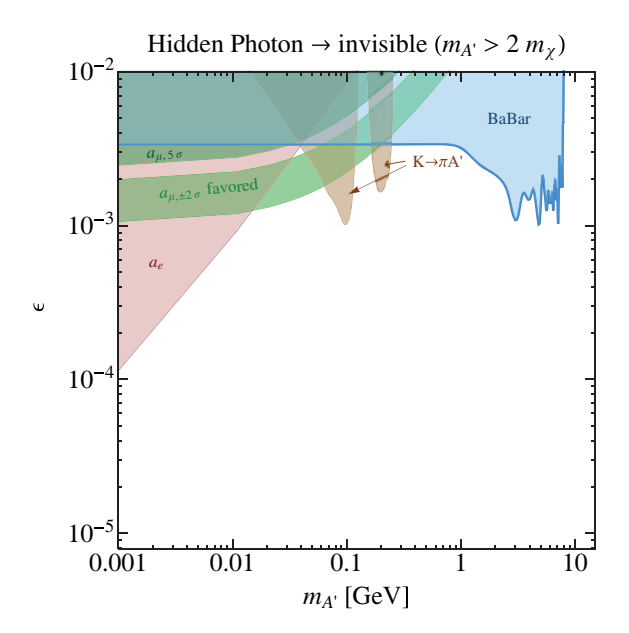


Fig. 23. – Exclusion limits for $A' \to \chi \bar{\chi}$ through missing-mass searches.

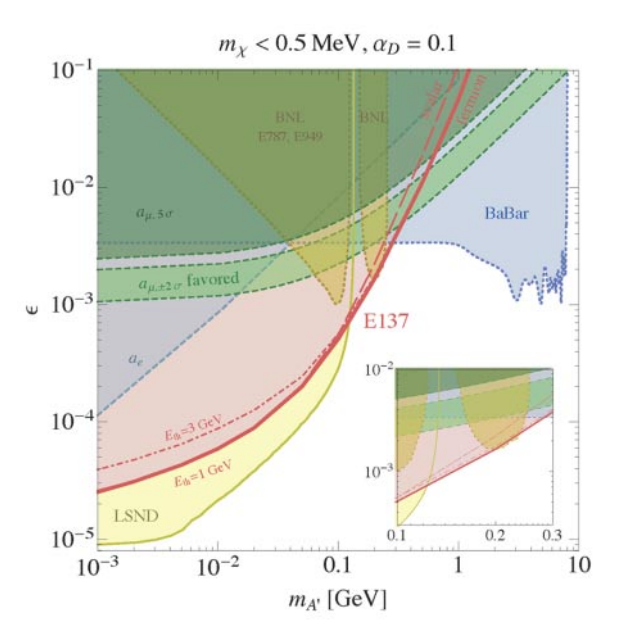


Fig. 24. – Exclusion limits for $A' \to \chi \bar{\chi}$ through dark matter scattering process [71].

4.3.1. Dark matter scattering searches. The process under investigation consists of two steps described in fig. 25. A beam of dark matter particles χ is obtained through the decay of A' produced in a target through A'-strahlung process, fig. 25a). The mechanism of dark photon production is described by the parameters ϵ^2 and $M_{A'}$. The dark matter particles can traverse the beam dump due to their weak interaction with ordinary matter and can then be detected through their scattering with the nuclei in a dense downstream detector, fig. 25b).

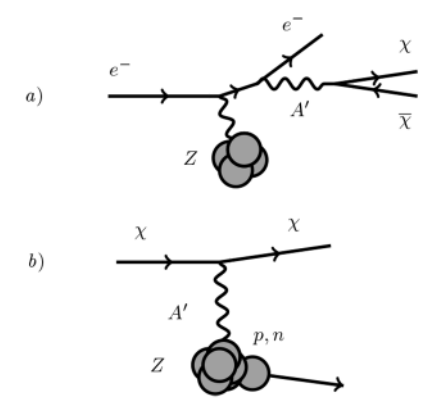


Fig. 25. – a) $\chi\chi$ pair production in electron-nucleus collisions. b) χ scattering off a detector nucleus and liberating a constituent nucleon.

If $m_{A'} < 2m_{\chi}$, the dominant χ production mechanism in an electron fixed-target experiment is the radiative process with an off-shell A'. In this regime, the χ production yield scales as $\sim \alpha_D \epsilon^2/m_\chi^2$. If $m_{A'} > 2m_\chi$, the secondary χ -beam arises from radiative A' production followed by $A' \to \chi \bar{\chi}$ decay. In this regime, the χ production is proportional to $\epsilon^2/m_{A'}^2$. The χ -nucleon scattering in the detector via A' exchange occurs with a rate proportional to $\alpha_D \epsilon^2 / 2m_{A'}^2$ over most of the mass range. The combination of the two steps leads to a suppression factor $\epsilon^4 \alpha_D/m_{A'}^4$ for the on-shell production, and therefore a very large number of primary particles are necessary. The only possible approach in this case is to dump an extremely intense beam on a high Z thick target. The A'strahlung production allows to reach high dark photon masses providing a high discovery potential to this technique. On the other hand, the four parameter space involved in the model limits somehow its exclusion power. Recently the results from E137 and LSND experiments were reinterpreted [71] in terms of this model leading to the exclusion limits in fig. 24, for the fixed values of $\alpha_D=0.1$ and $m_\chi<0.5\,\mathrm{MeV}.$ The Liquid Scintillator Neutrino Detector (LSND) was a scintillation counter at Los Alamos National Laboratory. It used a 800 MeV proton beam on two different targets over its lifetime, water and a high-Z metal. The experiment collected data from 1993 to 1998. The detector consisted of a tank filled with 167 tons of mineral oil and 6.4 kg of b-PDB organic scintillator material. The Cherenkov light emitted by interactions of the particles was detected by an array of 1220 photomultiplier tubes. LSND sets a strong constraint (yellow region/solid line) [71] if A' interacts with both electrons and quarks (as it would for the kinetic mixing model, but not for example in the case of a leptophilic mediator). Here χ is produced through the cascade decays of neutral pions produced in the proton-target collisions, $\pi^0 \to \gamma A'$ with $A' \to \chi \bar{\chi}$, and detected via its scattering with electrons. For the computation of the detector acceptance all the results of the scattering exclusions, shown in fig. 24, rely on the additional assumption that in the dark sector there is just a single stable state χ lighter than the A'. If this is not the case the exclusion limits may look rather different.

- 4°3.2. Searches for the dark photon at MiniBooNe. A proposal to search for dark matter at MiniBooNe was submitted to FNAL Pac at the end of 2013. The collaboration requested run time to collect a total of $2\cdot 10^{20}$ protons on target (POT) in beam off target mode [72]. The dominant production mode of dark matter particles at MiniBooNe is decays of the mediator particles created by decays of neutral mesons. The dark matter particles can be also produced through direct collisions of the beam protons in the dump. The accessible phase space to the MiniBooNe dark matter search is shown in fig. 26. Here, on the x-axis is the dark photon mass, and on the y-axis is the kinetic mixing parameter ϵ , assuming the dark matter mass $m_{\chi}=10\,\mathrm{MeV}$ and the gauge coupling $\alpha_D=0.1$. MiniBooNe exclusion region can be seen in green. The experiment collected $1.86\cdot 10^{20}$ POT during a 10 month run in beam off target mode to reduce the neutrino background. Preliminary analysis using 17% of the data is ongoing to tune the background evaluation. First results are expected towards the end of 2015.
- 4.3.3. Missing-mass-based searches. The missing-mass technique is based on the direct detection of the A' through the measurement of its mass as a missing mass in kinematically constrained final states. Ignoring the decay products of the A', the exclusions provided by this technique can be described with a simplified model using only ϵ^2 and $M_{A'}$ parameters. The production of the A' through e^+e^- annihilation limits the accessible mass region for low energy colliders [73, 74] while the use of meson decays limits

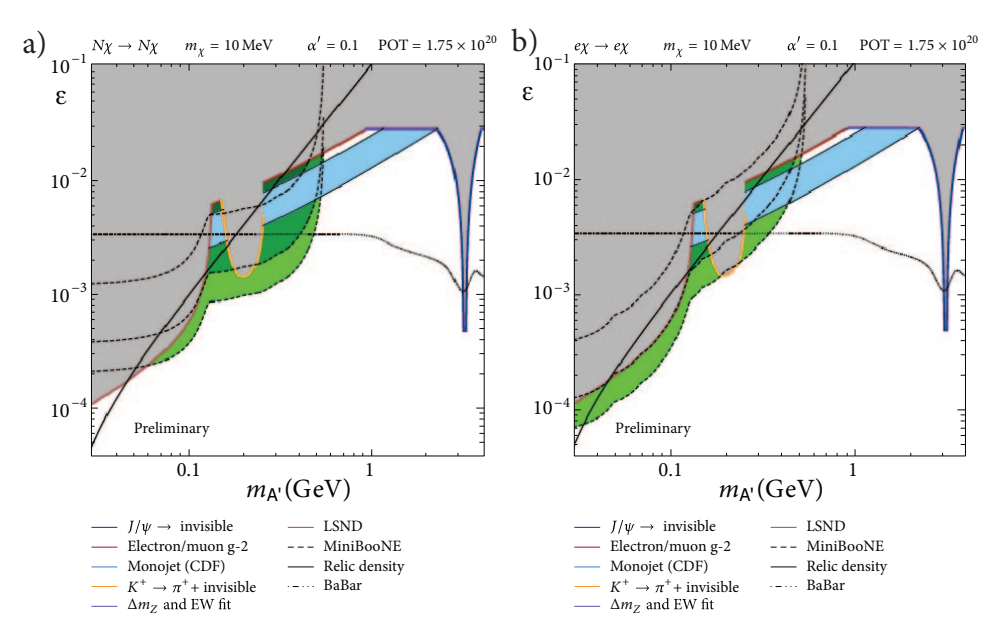


Fig. 26. – a) MiniBooNe expectation for χ -nucleus scattering collisions. b) MiniBooNe expectation for χ -electron scattering collisions [72].

the statistical sensitivity due to the relevant meson production cross-section. Recently, invisible experiments based on missing energy detection in bremsstrahlung production have been proposed as well [75]. In the eN interaction the recoiling nucleus usually takes a small part of the beam energy and the largest fraction of it is carried by the dark photon. After A' decays into $\chi\chi$ the signature will be the observation of an electron with a small energy, measured in an electromagnetic calorimeter. The dominant irreducible background is represented by events with neutrinos in the final state, like for example the charge current exchange $eN \to N'\nu$, with an addition shower in the calorimeter originating from bremsstrahlung photons or scattered electrons. In addition, the detector should be extremely efficient (hermetic) in detecting all visible particles in the final state. The exclusion limits obtained in [75] are impressive even if the proposed technique appears to be very challenging from an experimental point of view.

The only limit coming from experimental search present in fig. 23 comes from a preliminary result presented by by BaBar [76] at ICHEP 2008, recently reinterpreted in terms of dark photon exclusion in [77]. BaBar collaboration performed a bump hunt search for a light scalar particle produced in single-photon decays of the $\Upsilon(3S)$ resonance through the process $\Upsilon(3S) \to \gamma + A^0$, $A^0 \to \text{invisible using a data sample collected with a single photon trigger. They found no evidence for such processes in a sample of <math>122 \cdot 10^6$ $\Upsilon(3S)$ decays setting a preliminary upper limit on its branching ratio in the mass range $M_A^0 < 7.8\,\text{GeV}$. Reinterpretation in terms of dark photon model led to the exclusion region in blue in fig. 23. Recently, a new effort started in the collaboration which might lead to the publication of the final result.

The BESIII experiment published a search for invisible decays of the η and η' mesons motivated by the possible existence of light neutral dark matter particles [78]. A sample of $J/\psi \to \phi \eta(\eta')$ and missing energy was selected by tagging the ϕ . No significant signal

was observed, and 90% C.L. limits on the branching ratio BR($\eta(\eta') \rightarrow$ invisible) were set. These bounds constrain the invisible dark photon decays through η (η') \rightarrow A'A', $A' \rightarrow$ invisible, and cover therefore very narrow region of the parameter space (see fig. 26).

4°3.4. Indirect limits. In both figs. 23 and 24 additional indirect limits are present. The limits coming from the muon (g-2) anomaly, described in sect. **3**, are still valid in case of invisible dark photon decays. In addition, bounds to dark photon invisible decays can be obtained from the process $K^{\pm} \to \pi^{\pm} A'$, with a rate given by [47]

$$\begin{split} \Gamma(K^{\pm} &\to \pi^{\pm} A') = \\ & \frac{\epsilon^2 \alpha W^2 m_{A'}^2}{2^{10} \pi^4 m_K^7} \sqrt{\lambda(m_K^2, m_\pi^2, m_{A'}^2)} [(m_K^2 - m_\pi^2)^2 - m_{A'}^2 (2m_K^2 - 2m_\pi^2) - m_{A'}^2], \end{split}$$

where W is a function given in ref. [48]. The measurement of $\mathrm{BR}(K^+ \to \pi^+ \nu \bar{\nu})$ [79] by the BNL experiments E949 and E787 was used to derive the upper bound for the $\mathrm{BR}(K^\pm \to \pi^\pm A')$ process. The CERN NA62 experiment [80] will improve the sensitivity in this channel by measuring $\mathrm{BR}(K^+ \to \pi^+ \nu \bar{\nu})$ with a 10% precision. These kinds of limits are however model dependent. In fact, if a Z-A' mass mixing with the Standard Model Z-boson is introduced, the bounds from $K \to \pi + \mathrm{nothing}$ can be weakened up to a factor of ~ 7 as pointed out in [47].

5. - Future dark photon searches

Exploring the existence of a dark sector and of its constituents, new light weakly interacting particles, will be an important challenge for the particle physics in the next decade. The search for dark photon is strongly motivated by the attempt to understand the nature of the Dark matter and its interaction with Standard Model particles. Some of the existing facilities around the world are well suited for these searches. With modest investments in dedicated experiments opportunities for revolutionary discoveries are offered to low energy accelerators as well. Nevertheless the region of parameter space left for observation involves very low couplings requiring high luminosity machines and high rate capable detectors. A rich, diverse, and low-cost experimental program with a high discovery potential is already planned or proposed for the next few year (see fig. 7).

- 5.1. Experiments devoted to visible dark photon decays. Despite the fact that the region preferred by muon $(g_{\mu}-2)$ has been recently completely covered, the interest in searching for dark photon decaying into Standard Model particles is still high since a large part of the parameter space is yet unexplored. In fact, although the opportunity to explain the present muon g-2 anomaly through the dark photon was an exciting perspective, there are still many SM anomalies that can be clarified by dark sector models and therefore the physics case for dark photon searches with "visible" decay technique is still very clear. For this reason several laboratories are planning to explore dark photon parameter space with dedicated experiments in the next decade.
- 5.1.1. The HPS experiment. HPS is a fixed-target experiment running in the experimental Hall B of the Thomas Jefferson National Accelerator Facility (JLab) [81], using the CEBAF high-intensity electron beam. The beam, impinging on a thin $(0.25\%X_0)$

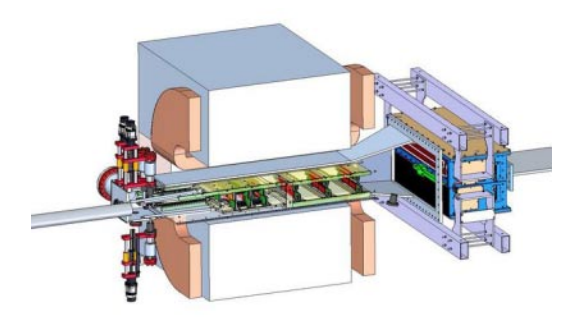


Fig. 27. – Layout of the HPS experimental setup.

Tungsten target foil, can produce dark photons through A'-strahlung, and the A' can then decay to e^+e^- . By reconstructing the momenta of the two charged particles HPS will search for a narrow resonance in the invariant-mass spectrum over the quantum electrodynamics (QED) background. Moreover, depending on $M_{A'}$ and ϵ , the dark photon can be long-lived, producing a distinct secondary decay vertex detached from the target. HPS will also use this signature to distinguish the signal from the QED pairs produced promptly in the target. The HPS detector setup is shown in fig. 27. It is made of a $\sim 1\,\mathrm{m}$ long Silicon Vertex Tracker (SVT) inside an analysing dipole magnet, to reconstruct charged particle trajectories and vertices, and a fast lead-tungstate electromagnetic calorimeter (ECal) to measure particle energies, identify e^+e^- pairs, and generate the trigger for the experiment.

The HPS reach was computed by assuming a one-week run at 1.1 GeV, a one-week run at 2.2 GeV, and a two-week run at 4.4 GeV. The two yellow lines in the reach plot in fig. 28 correspond to the two different analysis techniques used in HPS: the resonance

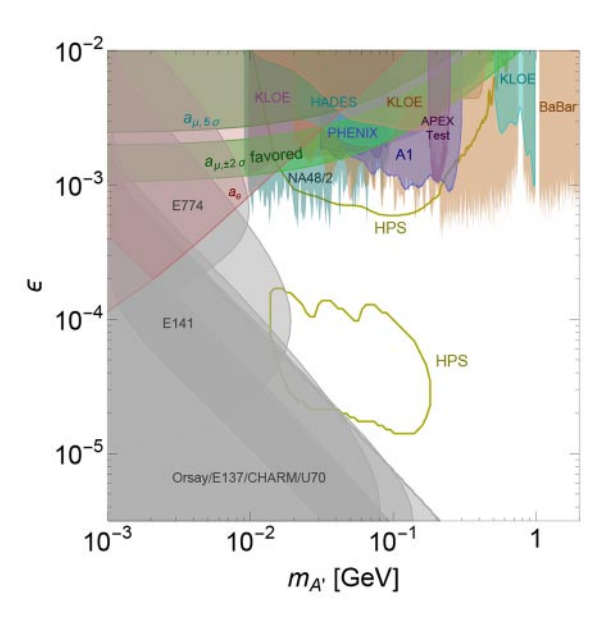


Fig. 28. – HPS expected exclusion limits. The continuous yellow line corresponds to the 2σ limit.

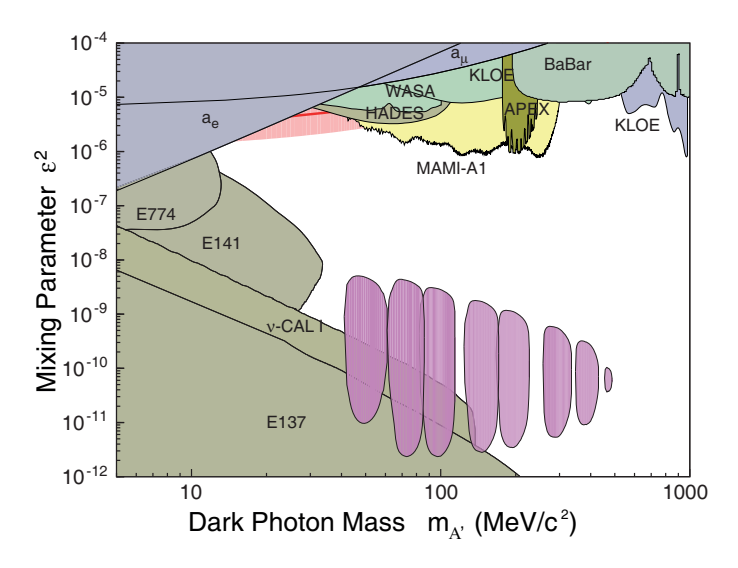


Fig. 29. – Expected reach for displaced vertex technique at MAMI, shown in pink [82].

search at higher ϵ^2 and detached vertex search at lower ϵ^2 . Even if the region of parameter space accessible using the resonance search technique has been mostly covered by other experiment, the detached vertex technique will allow HPS to access a large unexplored region which is hard to be reached by both colliders and beam dump experiments [81]. HPS is already installed in Hall B at JLAB and completed a successful engineering run during spring 2015. The experiment has currently finished its first data taking collecting roughly 1/3 of a week of data at 1.1 GeV with nominal detector configuration. Data analysis is ongoing and first physics results are expected within the end of the year.

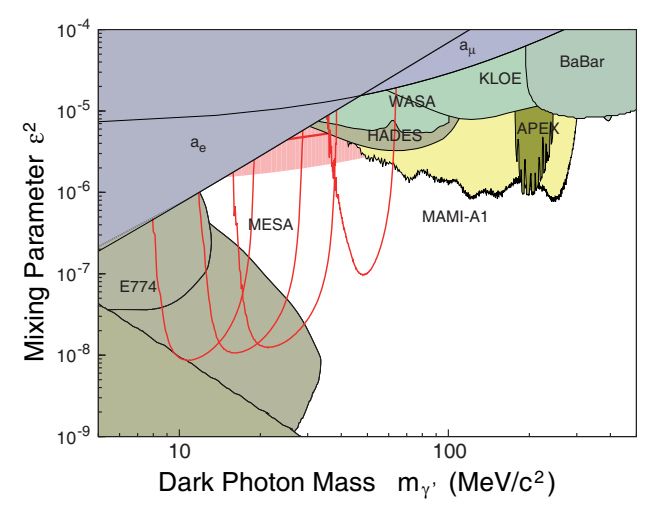


Fig. 30. – Expected reach, shown with red curves, for dark photon searches at MESA.

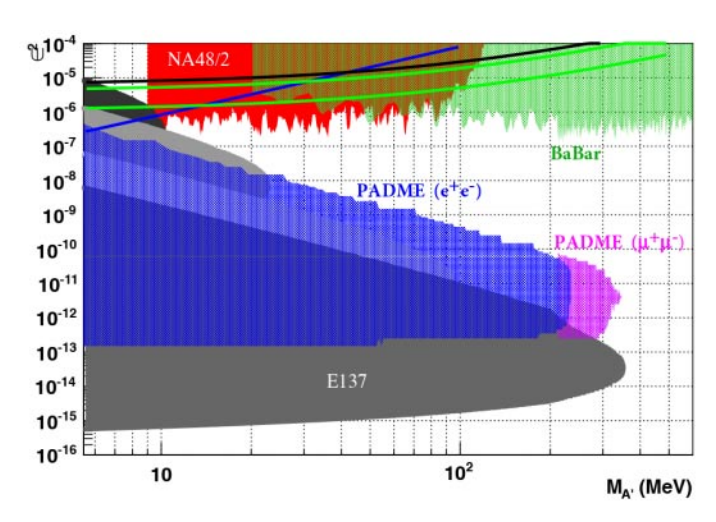


Fig. 31. – Preliminary estimate of a dump experiment at the Frascati Linac.

 $5^{\circ}1.2$. MAMI and MESA. The accelerator complex at the Mainz Microtron (MAMI) has already produced valuable results in dark photon searches by using the A1 spectrometer. The A1 collaboration is currently working on the upgrade of the interaction region to allow the A1 experiment to be sensitive to displaced vertex events. The new region of the parameter space accessible with such a technique, according to preliminary studies, is shown in fig. 29. A test run was performed in 2013, showing that an optimized shielding of the production vertex was necessary in order to access the pink region in fig. 29 [82]. In the next few years the construction of a new machine is foreseen in the MAMI complex. The MESA (Mainz Energy-Recovering Superconducting Accelerator) machine will be a superconducting energy recovering accelerator operating at a maximum energy of 155 MeV after extraction. A pair of high resolution spectrometers will complete the experimental equipment. The new setup will be ideal to probe the mass region below $50 \, \mathrm{MeV}/c^2$ which cannot be reached by current setup. Expected exclusion limits for the MESA spectrometers are shown in fig. 30.

5.1.3. PADME dump at LNF. Recent study on the high-current operation of the DAΦNE linac at the Laboratori Nazionali di Frascati revealed the possibility to operate the machine in the regime of $\sim 2 \cdot 10^{20}$ electrons-on-target per year [83]. The PADME (Positron Annihilation into Dark Matter Experiment) collaboration evaluated the possible physics reach of a 1 year beam dump experiment with 1.2 GeV electrons using the PADME spectrometer to detect electron and muon pairs produced in dark photon decays behind a 10 cm tungsten dump. The experiment aims for a bump hunt search in the spectrum of reconstructed $m_{e^+e^-}$ or $m_{\mu^+\mu^-}$ originating from dark photon decays downstream of the dump. The preliminary results show the potential to explore a region of couplings between 10^{-4} and 10^{-6} for masses in the range 20–300 MeV/ c^2 [84]. Figure 31 shows the preliminary estimate for a zero background dump experiment able to detect dark photon decaying to either e^+e^- or $\mu^+\mu^-$ pair. The actual running of such an experiments requires some infrastructural work to be carried out at the DAΦNE complex. Possible time scale of this project is at present unknown.

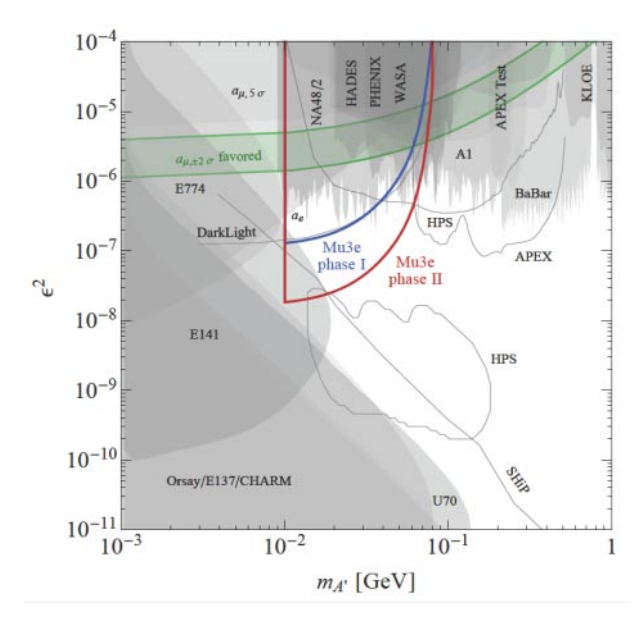


Fig. 32. – Estimated exclusion limits for a mu3e like experiment [85].

5.1.4. NA62 at CERN. The NA62 experiment is currently taking data at CERN SpS [80] to measure the branching fraction of the $K^+ \to \pi^+ \nu \bar{\nu}$ decay with a precision of 10%. The experiment will accumulate an unprecedented amount of K^+ and π decays using $\sim 10^{19}$ proton on a beryllium target. The collaboration is considering several possibilities to constrain the dark sector models: displaced vertices technique, decay products of π^0 s originating from kaon, η , and D decays, and proton bremsstrahlung production at the target. The improved measurement of the BR($K^+ \to \pi^+ \nu \bar{\nu}$) could be used as well to constrain the A' invisible decays, as described in [47].

5.1.5. Mu3e at PSI. A recent study [85] demonstrated that the upcoming Mu3e experiment at the Paul Scherrer Institute (PSI) in Switzerland is also sensitive to dark photons. Using an unprecedented number of muon decays in their search for the lepton flavour violating decay $\mu^+ \to e^+ e^- e^+$, Mu3e can also look for the decay $\mu^+ \to e^+ A'$, $A' \to e^- e^+$. The A' could be produced by radiation either from the muon or the electron or by an off-shell W^+ [85]. During its first phase, Mu3e will collect 10^{15} muon decays, and more than $5.5 \cdot 10^{16}$ muon decays by the end of phase II using the high intensity PSI proton beam of 2.2 mA at 590 MeV/s. To achieve the required sensitivity, a novel design based on high-granularity thin silicon pixel detectors supplemented by a fast timing system was proposed. For $m_{A'} < 2m_{\mu}$, the dominant decay is to electron positron pairs with invariant mass equal $m_{A'}$. The invariant-mass spectrum is dominated by SM background events, but a resonance search can be used to isolate the dark photon signal. In addition, displaced e^+e^- vertices can also be used to probe long-lived dark photons. The signal sensitivity is estimated by fitting a signal component on top of the expected background in the range $10 \,\mathrm{MeV} < m_{A'} < 80 \,\mathrm{MeV}$. Each fit is performed over an interval of $\pm 5 \,\mathrm{MeV}$ around the nominal dark photon mass. Confidence level limit on the number of signal events is estimated and a bound on the $\mu^+ \to e^+ A'$, $A' \to e^- e^+$ branching fraction is derived by dividing by the signal efficiency and the number of muon decays.

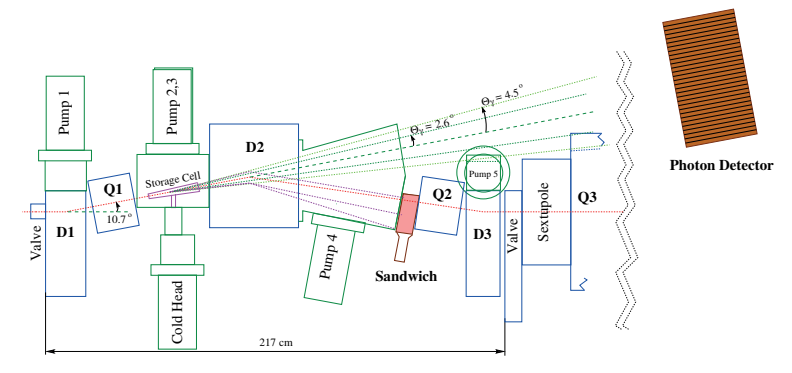


Fig. 33. – Layout of the VEPP-3 experimental setup.

These results are translated into accessible limits on the kinetic mixing parameter shown as a blue (red) solid line for Mu3e phase I (II) in fig. 32. The Mu3e construction will be completed in 2016 and the experiment plans to start the phase I data taking in 2017.

5.2. Searches sensitive to invisible decays. – Following the publication of the dark photon search by NA48/2, which completed the effort to constrain the region preferred by the muon $(g_{\mu}-2)$ anomaly in the hypothesis of dark photon decay to SM particles only, new attention has been devoted to "invisible decays" models both theoretically and experimentally. In fact, if the A' decays to dark sector particles, almost all of the available experimental constraints can be evaded and the dark photon is still a valuable explanation for the muon (g-2) anomaly. Due to the weak experimental signature, the search for invisibly decaying dark photon requires carefully designed dedicated experiment. Thanks to the rich phenomenology of the dark sector, the combined effort of several machines and different experimental techniques could provide access to the whole region of interest solving the muon (g-2) anomaly already in the next decade.

5.2.1. VEPP3. The first experimental proposal to search for the dark photon in $e^+e^$ annihilation is described in [73]. The search method is based on a missing-mass spectra in the reaction $e^+e^- \to \gamma A'$ using a positron beam incident on a gas hydrogen target, internal to the VEPP-3 storage ring. It allows the observation of the A' signal independently of its decay modes and life time. The nominal luminosity of 10³² cm⁻² s⁻¹ is routinely achieved and an improvement of a factor 5-10 is expected in the near future. In a six-month run the total accumulated statistics will be $3.5 \cdot 10^{11}$ events, assuming a time efficiency of 75%. In fig. 33 a top view of the VEPP-3 hall in the vicinity of the internal target equipment and the possible location of the photon detector are shown. In the VEPP-3 proposal there is no definite solution for the calorimeter but a combination of the PRIMEX and the CLEO-II dismissed calorimeters placed at an 8 m distance from the target is proposed. To reject the main background coming from photons emitted by bremsstrahlung in the target a positron veto is placed in front of Q2 (see fig. 33). The veto collects the positron deflected by the dipole D2 due to their energy loss associated with the emission of the radiated photon. The detector, composed of a sandwich of tungsten and plastic scintillators is divided in two parts, to avoid crossing the beam plane region where the rate of radiated photons is extremely high. The veto is expected to provide

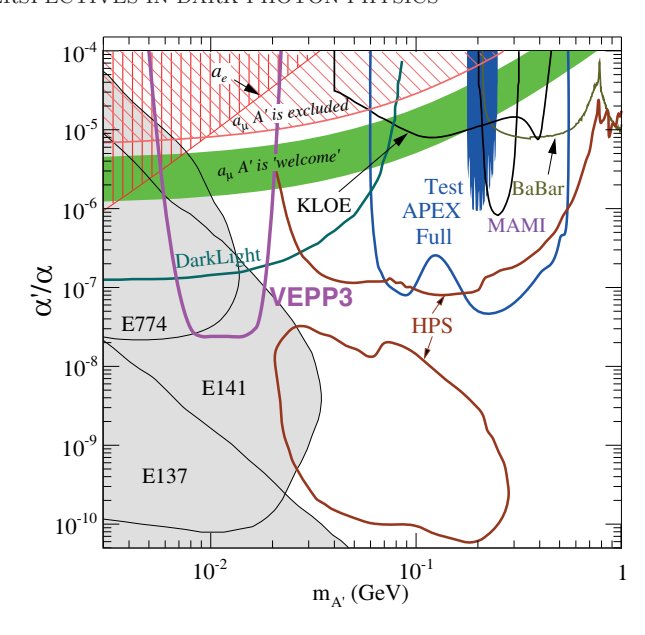


Fig. 34. – VEPP-3 expected exclusion limits in the invisible channel [73].

a rejection factor of 50 for the bremsstrahlung background. A preliminary study of the sensitivity based on calculations using a benchmark mass of $15 \,\mathrm{MeV}$ for the A' allowed to identify the region which will be accessible to the VEPP-3 experiment (see fig. 34).

5°2.2. PADME at LNF. The PADME experiment [74,86] aims at dark photon search using the 550 MeV positron beam provided by the DAΦNE linac at the INFN Laboratori Nazionali di Frascati impinging on a thin target. The process of interest is $e^+e^- \to \gamma A'$ where the positrons are the beam particles and e^- are the electrons in the target. The accompanying SM photon 4-momentum is measured by a calorimeter regardless of the A' decay products. A single kinematic variable characterising the process, the missing mass, is computed using the formula $M_{\rm miss}^2 = (P_e + P_{\rm beam} - P_{\gamma})^2$. Its distribution should peak at $M_{A'}^2$ for dark photon decays, at zero for the concurrent $e^+e^- \to \gamma\gamma$ process, and should be smooth for the remaining background. The experiment is composed of a diamond target to measure the average position and the intensity of the beam bunch by bunch, a spectrometer immersed in the field of a dipole magnet to deflect the positron beam and to measure the charged particle momenta, and an electromagnetic calorimeter to measure/veto final state photons. The apparatus is inserted into a vacuum chamber to minimize the unwanted interactions of the primary and the secondary particles with the air. A preliminary drawing of the experimental setup is shown in fig. 35.

Four different types of dark photon searches are in principle accessible by combining production processes and decay final states: annihilation-produced dark photon decaying into dark sector particles or into e^+e^- pairs, bremsstrahlung-produced dark photon decaying into dark sector particles or into e^+e^- pairs. The present Frascati linac maximum positron energy of 550 MeV allows the production of dark photons through annihilation up to a mass of 23.7 MeV, while an upgrade to 750 MeV of the DA Φ NE linac would allow to reach $M_{A'} \sim 27.7$ MeV. Detailed studies have been performed only for annihilation production to assess the sensitivity to invisible decays. Studies on the other final

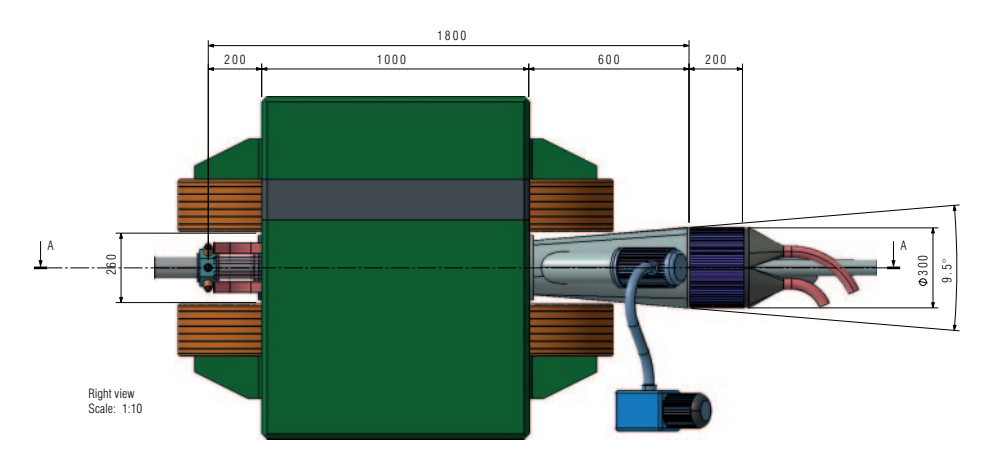


Fig. 35. – Lateral view of the PADME experimental setup.

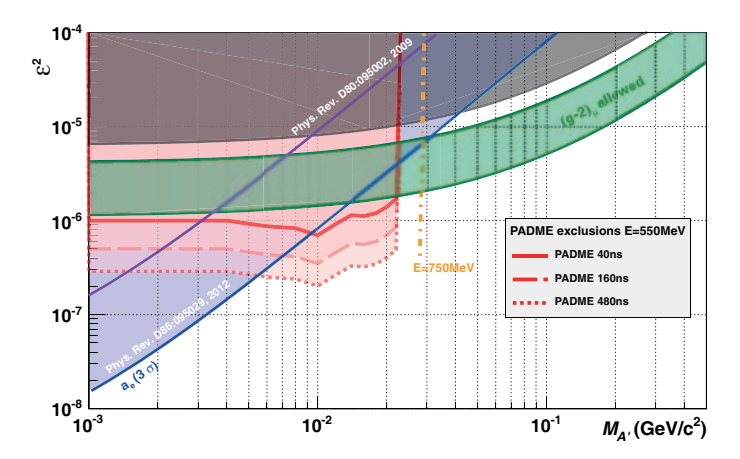


Fig. 36. – Expected PADME exclusion limits in the invisible channel $A' \to \chi \bar{\chi}$ [87].

states are ongoing. The sensitivity of the experiment was estimated assuming one year of running with 60% efficiency, a constant positron flux and different bunch lengths, as indicated in fig. 36, corresponding to about $1 \cdot 10^{13}$, $3 \cdot 10^{13}$, and $1 \cdot 10^{14}$ positrons on target respectively. Under the assumption of no signal, an upper limit on the dark photon coupling ϵ can be set, using the statistical uncertainty on the simulated background. The result shown in fig. 36 applies to both visible and invisible dark photon decays, since the event selection includes both cases. PADME sensitivity to visible decays of bremsstrahlung-generated dark photon is under investigation. The PADME search for new low mass mediators is completely general, in particular in the "invisible" case. Therefore the experiment will be sensitive to any new small mass particle, like low mass dark Higgs or leptophilic gauge bosons, produced in e^+e^- collisions. The PADME experiment has been included in the INFN "Proposal for a long term strategy for accelerator based experiments" [87] and has been recently financed for a research and development phase. The collaboration is aiming for a first physics run in early 2018.

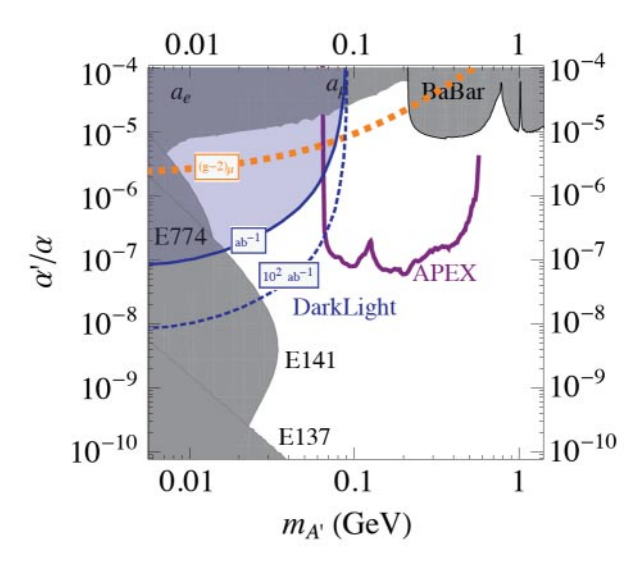


Fig. 37. – Sensitivity reach of the Dark Light experiment for integrated luminosities of $1\,\mathrm{ab^{-1}}$ and $100\,\mathrm{ab^{-1}}$.

 $5^{\circ}2.3$. DarkLight experiment. DarkLight experiment will be located at Jefferson Laboratory [88] and will measure precisely the electron proton scattering. A 100 MeV high intenstity (5 mA) beam will interact with a molecular hydrogen target with thickness of $10^{19} \, \mathrm{cm}^{-2}$. No material separates the target volume from the beam vacuum chamber minimizing the expected background. All charged particles in the final state will be detected in a set of tracking gas and silicon detectors, which are located around the interaction region. A solenoidal magnet surrounds the experiment, providing 0.5 Tesla magnetic field.

The experiment is organized in two phases [89]. Phase I is mostly devoted to searches for A' decaying in e^+e^- , with e^- , p, and e^+e^- detected in the tracking system. Data taking is expected to start within an year.

Phase II of the experiment will be optimized also for the search of A' decaying to invisibles. This would require modification of the beam pipe and development of a novel readout technology to handle the enormous $O(100 \,\mathrm{MHz})$ event rate.

The expected reach in the dark photon parameter space is shown in fig. 37. In case of success of the experiment this search will cover one of the most difficult to access regions [90] $-10\,\mathrm{MeV} < M_{A'} < 80\,\mathrm{MeV}$ and $10^{-5} < \epsilon^2 < 10^{-7}$, with $1\,\mathrm{ab}^{-1}$ integrated luminosity.

5°2.4. Cornell. Recently a new proposal to search for the invisible decay of the dark photon was presented at Cornell's Wilson Laboratory [91]. The experiment proposed to search for the process $e^+e^- \to \gamma A'$ using a positron beam with energy in the range 4.7–5.3 GeV. The beam is extracted slowly from the CESR storage ring and interacts in a fixed beryllium target. The ordinary photon in the final state is observed and its four-momentum is measured by a segmented detector. The undetected A' will appear as a bump in the missing-mass spectrum. The experiment plans to use a calorimeter of CsI crystals. It will be located about 10 m downstream of the target and the crystals will be arranged in an annular configuration. They are recovered from the CLEO endcap calorimeters and are $5 \times 5 \times 30 \, \mathrm{cm}^3$ rectangular solids, well suited for stacking in simple arrays.

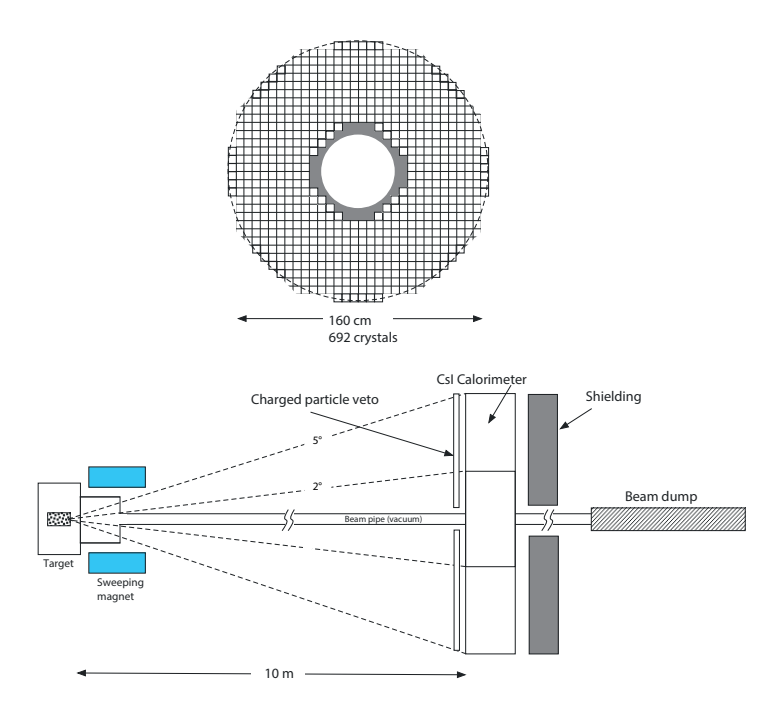


Fig. 38. – Layout of the Cornell experimental setup.

To assure an angular coverage in the range $2 \deg < \theta_{\gamma} < 5 \deg$ with respect to the primary beam the total number of crystals needed is about 700. As a precaution against charged particles that may reach the calorimeter, a set of scintillator slabs will cover its front face, and a sweeping magnet is located just after the target to remove low energy ones. Each slab is 5 cm wide, matching the crystal size, and the slabs are organized in both horizontal (x) and vertical (y) groups so a single crystal can be vetoed by an xy coincidence. The non-interacting beam positrons are absorbed in a beam dump located downstream of the calorimeter. The planned detector configuration is illustrated in fig. 38.

The Cornell experiment will probe values of ϵ in the range 10^{-3} – 10^{-4} in the kinematically accessible dark photon mass window, provided by the 5 GeV positron beam (up to 70 MeV). The expected performance of the experiment, based on GEANT4 simulation and shown in fig. 39, indicates the region of the parameter space of coupling constant *versus* mass that this experiment can exclude with a run of 10^7 seconds. The collaboration is currently looking for a financial support.

5.2.5. BDX at JLAB. In the BDX experiment [92], a $O(\mathrm{m}^3)$ calorimeter will be installed behind one of the Jefferson Laboratory high intensity experimental Halls (A and C). High energy (11 GeV) electrons from the CEBAF accelerator will impinge on the beam dump, possibly producing a secondary dark matter beam. Dark matter particles will be detected through the scattering on the detector material (electrons and quasi free nucleons), resulting in a visible energy deposition (see fig. 40 for schematics of the experiment). In the foreseen setup, the $O(\mathrm{m}^3)$ detector is placed downstream with respect to the beam dump and is surrounded by an active veto system and by passive shielding to reduce the number of hits due to cosmogenic backgrounds (muons and energetic neutrons).

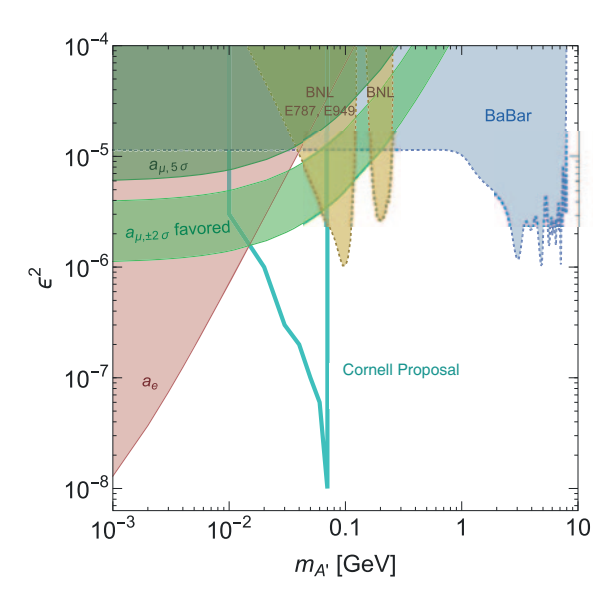


Fig. 39. – Expected exclusion in the invisible channel for the Cornell proposal.

The BDX experiment reach was computed by evaluating the foreseen number of background hits in the detector through detailed Monte Carlo simulations, and comparing this to the expected number of signal events (as a function of the model parameters). Red curves in fig. 41 show 10, 100, and 1000 event BDX yield projections for a kinetically mixed dark-photon (A') coupled to a nearly invisible fermion χ in the quasi-elastic nucleon recoil channel with 10^{22} EOT. Similar sensitivity can be achieved in the electron recoil channel giving to BDX the unique capability of being sensitive to different DM interaction mechanisms at the same time. The region potentially covered by using the JLab beam would therefore extend significantly the parameter space already excluded by previous experiments. A Letter of Intent [92] was submitted to PAC 42 of the Jefferson Laboratory in 2013. The collaboration was encouraged to perform further studies and to produce a Technical Design Report, expected for the end of 2015.

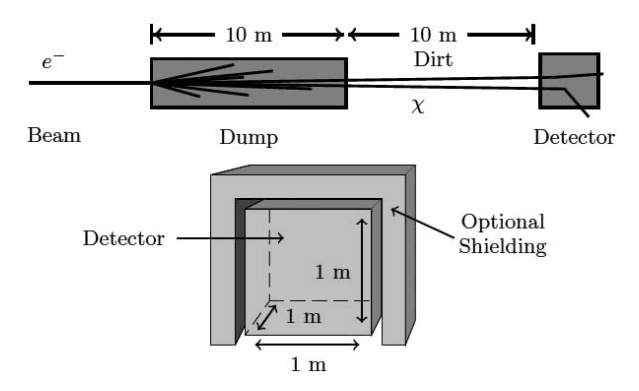


Fig. 40. – Schematic of the BDX experimental setup.

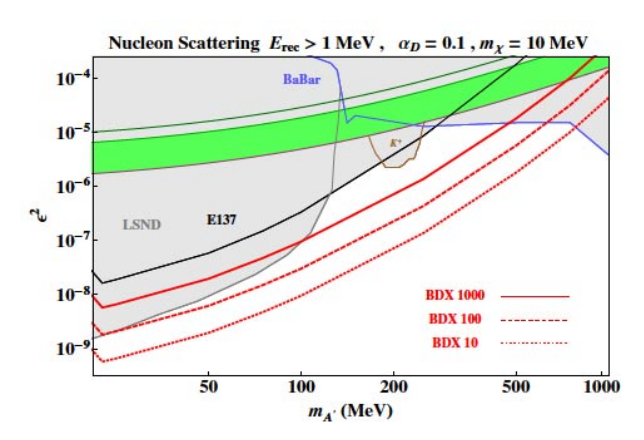


Fig. 41. – Expected exclusion in the invisible channel for the BDX proposal for $\alpha_D=0.1$ and $m_\chi=10\,\mathrm{MeV}.$

 $5^{\circ}2.6$. P348. A recently proposed experiment at CERN SPS [93] would also search for invisible A' decays. The experiment employs an innovative technique, by having the primarily e^- beam from the H4 line at SPS, with energy between 10 and 300 GeV, impinging on an active beam dump, made by a calorimeter based on scintillating fibres and tungsten, ECAL1. A nearly hermetic detector would be located behind the active beam dump. The detector is made by a charged particle veto counter, a decay volume, two scintillating fibre counters, a second electromagnetic calorimeter ECAL2, and a hadronic calorimeter. The experimental setup, shown in fig. 42, is optimized to search for visible A' decays. The expected sensitivity for different accumulated statistics is shown in fig. 43. The assumed beam energy is 30 GeV.

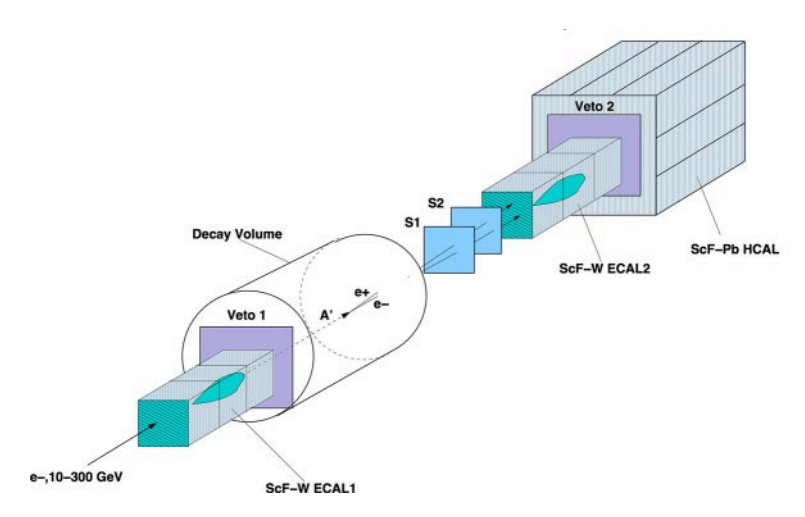


Fig. 42. – Layout of the P348 experimental setup [93].

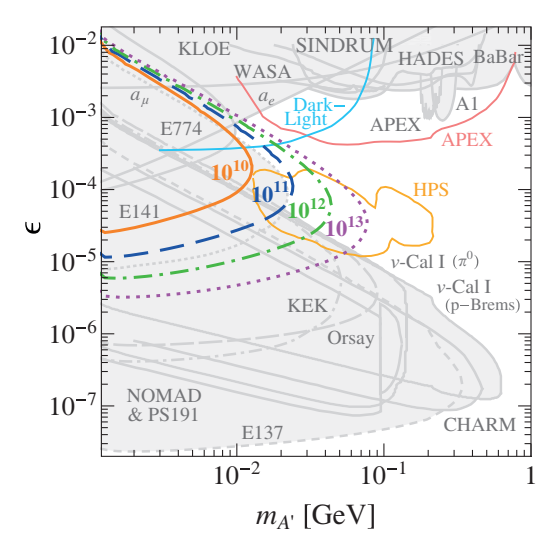


Fig. 43. – Expected 90% C.L. exclusion for different collected statistics of the P348 experiment [93].

The P348 experiment could also search for A' invisible decays by exploiting the detector hermeticity, and requiring a single hit in ECAL1 from the e^- radiating the A' with an energy lower than 10% of the primary beam energy. The projected sensitivity for $3 \cdot 10^{12}$ electrons on target covers a very large region in the dark photon parameter space, with $m_{A'} < 1 \, {\rm GeV}$ and $\epsilon > 1 \cdot 10^{-5}$ (see fig. 44). The orange and green lines show

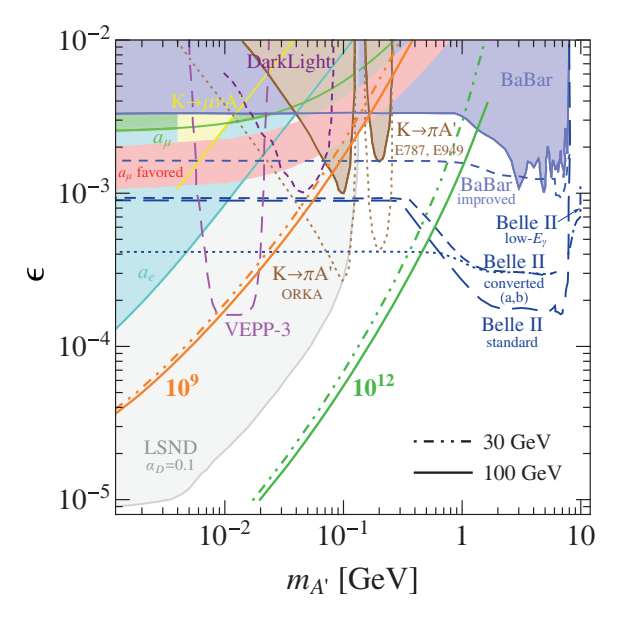


Fig. 44. – Expected exclusion in the invisible channel for the P348 proposal and for the Belle II experiment.

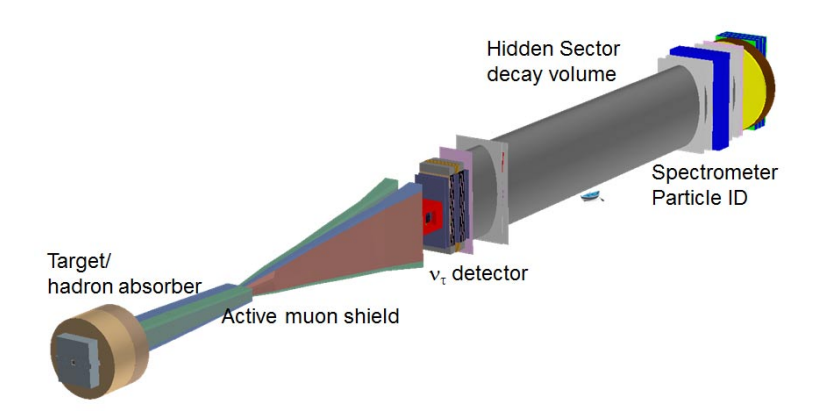


Fig. 45. – Overview of the proposed dump target and detector setup of the SHiP experiment.

the expected 90% C.L. exclusion areas corresponding, respectively, to 10^9 and 10^{12} accumulated electrons at 30 GeV (dash-dotted) and 100 GeV (solid) for the background-free case. To accumulate the required number of electrons a data taking period of at least 3 months is requested. Recent reanalysis [75] of the physics potential of P348 reports that the signal yield estimate at 90% C.L. exclusion is ~ 20 –30 times lower than what is inferred from fig. 44. In the event of a positive signal, the experiment would carve out a contour in the parameter space, but would not independently measure the A' properties. The experiment will have its first test run in the end of 2015 at H4 line at SPS to study beam related background.

5.2.7. Belle II at KEK. Belle II experiment at the SuperKEKB collider is a major upgrade of the Belle experiment at the KEKB asymmetric e^+e^- collider at the KEK laboratory in Japan. The upgrade of the new B-factory SuperKEKB, with a designed luminosity of $8 \cdot 10^{35}$ cm⁻² s⁻¹, is almost finished. The Belle II experiment will focus on the search for new physics beyond the Standard Model via high precision measurement of heavy flavour decays and search for rare signals. The upgraded detector will have about 35% better resolution in the dimuon invariant mass and the sensitivity to $A' \to l^+ l^$ decays can be improved [94]. This will be done through an implementation of a low multiplicity trigger. In addition, the collaboration is also investigating the possibility to implement a single photon trigger similar to the one used in BaBar [76] to search for invisible decays of the A'. Due to the very high luminosity of the new machine the mono photon trigger will be an experimental challenge. No official statements are available on whether or not it will be implemented. Dedicated sensitivity estimates for the Belle II experimens do not exist yet and projections were obtained by scaling the BaBar results for both the dilepton [65] and the mono photon result [76]. Exclusion limits for invisible case are shown in fig. 44. First collision at the SuperKEKB are currently foreseen for mid 2017, while physics run is expected to start in October 2018.

 $5^{\circ}2.8$. SHiP at CERN. The SHiP (Search for Hiden Particles) collaboration proposed to perform a beam dump experiment placed at the SPS accelerator at CERN [95]. The experiment will be located in the North Area and the planned proton beam intensity will be 4.5×10^{19} protons on target per year. The experimental design is shown schematically in fig. 45.

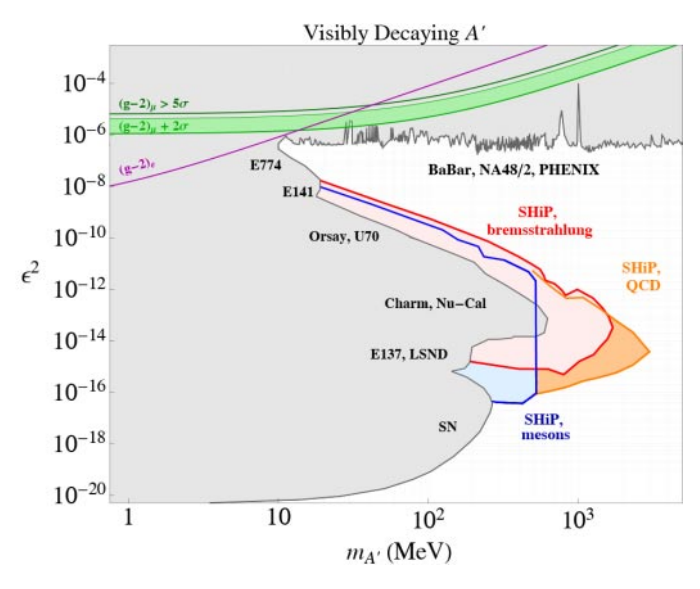


Fig. 46. – Projection of the exclusion limits in the dark photon parameter by the SHiP experiment [21].

The primary 400 GeV proton beam impinges on a tungsten target. A nominal spill intensity of 4×10^{13} protons on target is assumed for a total of 2×10^{20} protons on target in five years of operation. The target is followed by an active muon shield in a magnetic field. The detector complex could be divided into a neutrino detector followed by a setup devoted to the searches for particles from the hidden sector. The main goal of the tau neutrino detector is to perform the first direct observation of $\bar{\nu}_{\tau}$ and to measure the cross-sections for the 5.7×10^{15} $\bar{\nu}_{\tau}$ and ν_{τ} produced in the target. The hidden sector detector is located upstream of an evacuated decay volume followed by a magnetic spectrometer, timing detector, electromagnetic and hadron calorimeter and a muon detector, resembling a typical fixed-target experimental setup. The shielding and the long decay volume make the SHiP experiment perfect to search for any kind of light dark matter particles which live long enough and decay afterwards to SM particles.

Three modes of production are relevant for the projection of the SHiP sensitivity—meson decays, bremsstrahlung, and QCD production [34]. The QCD production was simulated with MadGraph5 [96]. The minimal detectable number of events was assumed to be N=3. The expected accessible region in $(\epsilon^2-M_{A'})$ plane to SHiP is shown in fig. 46. For first time masses up to $O(1\,\text{GeV})$ could be probed both through bremsstrahlung and QCD production mechanisms.

The existence of a neutrino detector close to the target could also provide possibility to detect dark photons even in the case when they do not decay predominantly to SM particles. This would imply the existence of light dark matter particles which are produced in the target and scatter in the downstream detectors. In the case of O(10 ton) detector and $M_\chi \ll M_{A'}$ the projected sensitivity of SHiP experiment is shown in fig. 47. The two red lines reflect the assumption of minimal detectable number of 1000 or 10 events. This might not be easy to achieve but even in such scenario the sensitivity is comparable to previous experiments.

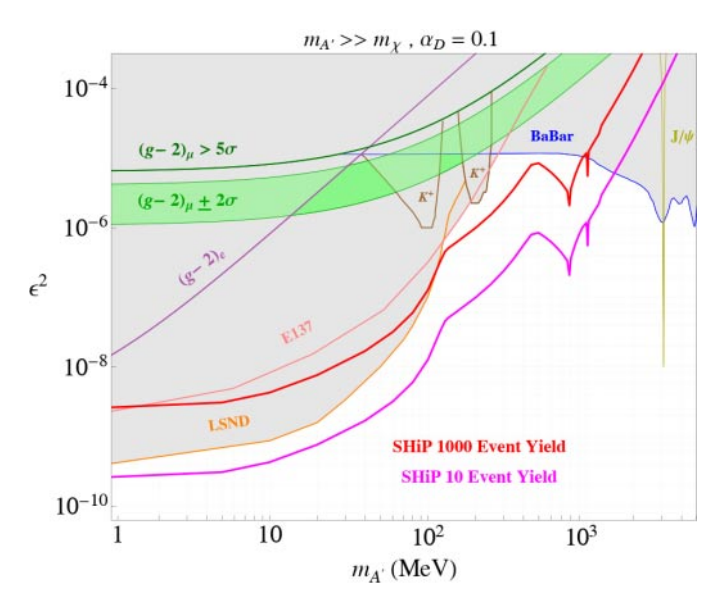


Fig. 47. – Exclusion limits by the SHiP experiment if the dark photon decays to invisibles [21].

6. - Constraints for non-minimal dark photon models

When the mass of the dark photon is not generated through the Stückelberg mechanism new couplings and interraction terms are necessary to account for it. This leads to the appearance of new production mechanisms and a new phenomenology of the processes and such models are usually classified as non-minimal. The dark photon mass can be inserted either by allowing the A' to interact with Standard Model Higgs or by introducing a new dark Higgs as a part of the dark sector. The first scenario has been recently extensively studied at the ATLAS and CMS experiments at LHC while the dark Higgs scenario has been constrained by KLOE, BABAR and Belle.

6.1. Searches through Higgs portal at LHC. – Searches for the dark photon at LHC are based on the hypothesis that the A' has an additional coupling to the SM Higgs and therefore a Higgs decay to dark photons is allowed. Both ATLAS and CMS had explored this possibility producing bounds on the mixing versus mass parameter space. The exclusion limits look rather impressive but the increasing number of assumptions in the model makes these bounds rather weaker than they appear. New searches are foreseen for LHC run II. Even if not strictly required by the minimal dark photon model, it is very important to probe the couplings of the dark photon with the Standard Model Higgs to get more understanding of the origin of the mass of the dark photon.

6.1.1. Search for dark photon at ATLAS. The search for displaced lepton jets recently published by the ATLAS experiment employed the full dataset collected during the 2012 run at $\sqrt{s} = 8 \text{ TeV}$, corresponding to an integrated luminosity of 20.3 fb⁻¹ [97].

Due to their small mass, A' are typically produced with a large boost at LHC and, due to their weak interactions, can have non-negligible lifetime. As a result from the dark photon decays, collimated jet-like structures might be expected, containing pairs of electrons and/or muons and/or charged pions ("lepton jets") that can be produced

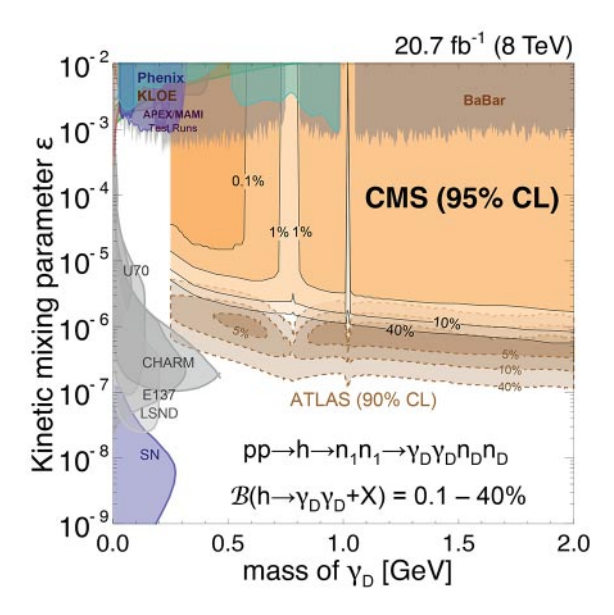


Fig. 48. – Limits by CMS on dark photon decaying into muon pairs through Higgs portal for different values of $BR(h \to 2A' + X)$ [98].

far from the primary interaction vertex of the event. The observed data were consistent with the background expectations. Limits were set on the $\sigma \times \mathrm{BR}$ for $h \to 2A' + X$ and $h \to 4A' + X$, for an A' mass of 0.4 GeV, as a function of the long-lived particle mean lifetime. Assuming the gluon fusion production cross-section for a SM Higgs boson, its branching fraction to hidden-sector photons is found to be below 10%, at 95% C.L., for hidden photons with $c\tau$ in the range 14 mm $\leq c\tau \leq$ 140 mm for the $h \to 2A' + X$ mode, and in the range 15 mm $\leq c\tau \leq$ 260 mm for the $h \to 4A'$ mode.

These results are also interpreted in the context of the Vector portal model as exclusion contours in the kinetic mixing parameter ϵ versus $m_{A'}$ mass plane (see fig. 48) and significantly improve the constraints from other experiments.

6.1.2. Search for dark photon at CMS. The CMS experiment recently presented a search for the pair production of new light bosons (A') decaying to pairs of isolated, oppositely charged muons (dimuons) [98]. A possible production mechanism for these new bosons is the decay chain of a Higgs boson, h, which can be SM-like or not: $h \to 2A' + X \to 4\mu + X$, where X denotes all other additional particles from cascade decays of the Higgs boson. A range of New Physics scenarios predicts such decay topology, including the next-to-minimal supersymmetric Standard Model (NMSSM) and models with hidden (or dark) sectors. In this models A' can have a substantial branching fraction into dimuon if its mass is in the range $2\mu < m_{A'} < 2m_{\tau}$ —the benchmark model for the CMS study. The CMS search was based on a data sample corresponding to an integrated luminosity of $20.7\,\mathrm{fb}^{-1}$ of proton-proton collisions at a centre-of-mass energy $\sqrt{s}=8\,\mathrm{TeV}$, recorded by the CMS detector in 2012. The data were collected with an online trigger selecting events containing at least two muon candidates. One event was observed in the signal region, with 2.2 ± 0.7 events expected from the SM backgrounds. 95% C.L. upper limits

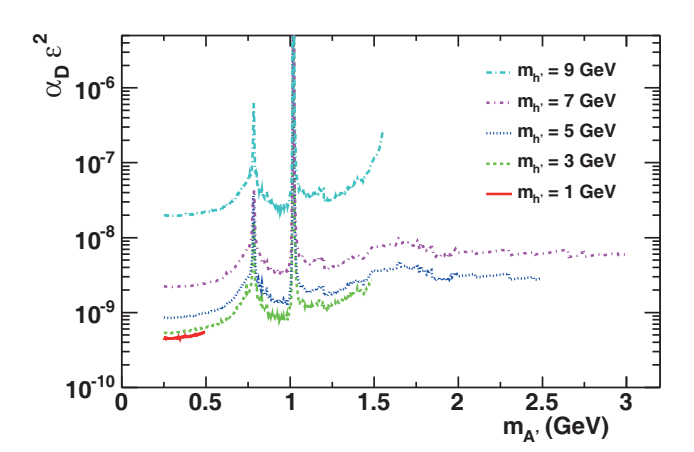


Fig. 49. – Limits on the dark photon parameters for different masses of the dark Higgs boson obtained from the searches for dark Higgs performed by the BaBar collaboration [99].

(black solid curves) from this search on $\sigma(pp \to h \to 2A' + X) \times \text{BR}(h \to 2A' + X)$ are shown in fig. 48 in the plane of two of the parameters (ϵ and $m_{A'}$) for the dark SUSY scenarios, along with constraints from other experiments. The coloured contours represent different values of $\text{BR}(h \to 2A' + X)$ in the range 0.1–40%.

6^{•2}. Searches for dark Higgs. – In models where the dark photon mass is generated through spontaneous symmetry breaking with a dark Higgs, an associate production of the dark Higgs and the dark photon is possible. Naturalness requires that the two particles have masses of the same order $m_{h'} \sim m_{A'}$. Most of the searches described below focus on this production channel and the results depend on the couplings in dark sector.

6[°]2.1. Search for dark Higgs at BaBar. BaBar collaboration performed a search for dark Higgs boson in the so-called Higgs-strahlung process

(54)
$$e^+ + e^- \rightarrow A'h'$$
, with $h' \rightarrow A'A'$,

which is possible for $m_{h'}>2m_{A'}$ and in the lack of other dark sector particles lighter than A'. The measurement was performed in the range $0.8\,\mathrm{GeV}< m_{h'}<10\,\mathrm{GeV}$ and $0.25< m_{A'}<3\,\mathrm{GeV}$. The search was performed with the fully reconstructed exclusive final states $3(l^+l^-)$, $2(l^+l^-)\pi^+\pi^-$, and $l^+l^-2(\pi^+\pi^-)$ or the partially reconstructed inclusive processes $2(\mu^+\mu^-)+X$ and $\mu^+\mu^-e^+e^-+X$, where X was any final state different from pions or leptons. The analysis for the inclusive processes was limited to $m_{A'}>1.2\,\mathrm{GeV}$.

The lack of extra signal provided limits to the $e^+ + e^- \to A'h', h' \to A'A'$ cross-section which was translated into 90% C.L. upper limit on the product of the dark coupling constant and the mixing parameter $\alpha_D \epsilon^2$. The results for the excluded region are shown in fig. 49 for different values of the dark Higgs boson mass. They assume prompt dark Higgs decay and prompt dark photon decay. The excluded range lies in the region $10^{-9} - 10^{-8}$ for $\alpha_D \epsilon^2$. In the assumption that $\alpha_D \sim \alpha_{\rm EM}$ the results could be translated into limits for ϵ^2 in the range $10^{-7} - 10^{-6}$ for the interval $0.25~{\rm GeV} < m_{A'} < 3~{\rm GeV}$. However those exclusions depend on the extra parameters $m_{h'}$ and α_D .

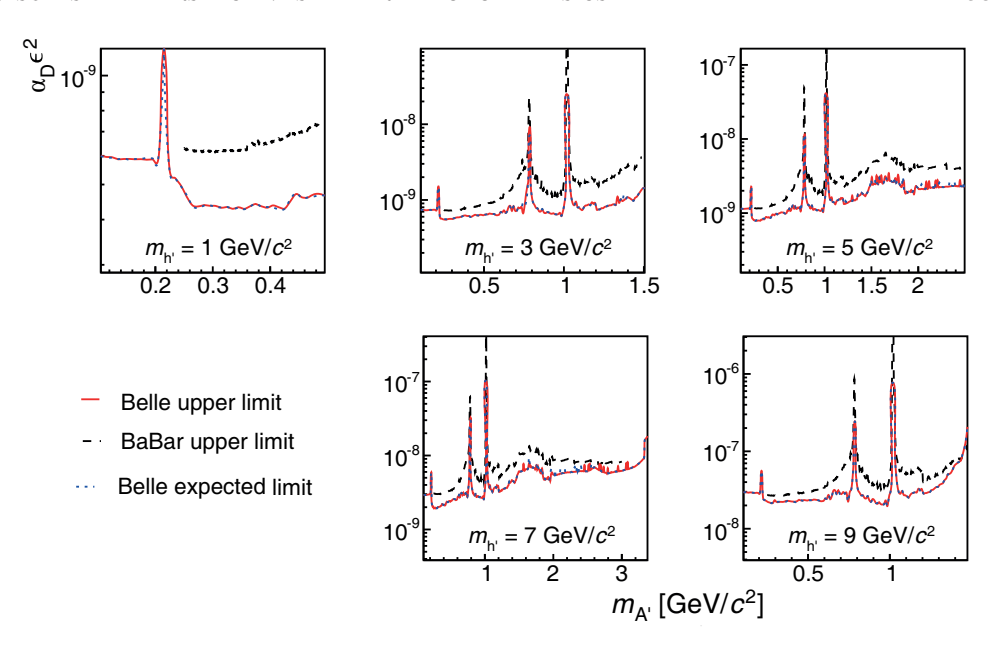


Fig. 50. – Excluded regions in the α_D - $M_{A'}$ parameter space for different masses of the dark Higgs boson [101].

6.2.2. Search for dark Higgs at Belle. The searches for dark Higgs at Belle were performed in analogous way to those at BaBar. The production and decay process of the dark Higgs boson was as described in eq. (54). Ten exclusive final states with $A \to e^+e^-$, $\mu^+\mu^-$, or $\pi^+\pi^-$ and three inclusive final states e^+e^-X , $2\mu^+\mu^-X$, and $e^+e^-\mu^+\mu^-X$ were investigated, where X denotes a dark photon detected through the missing-mass technique.

The data analysis was performed with the entire set of Belle data (977 fb⁻¹) in the interval $0.1\,\mathrm{GeV} < m_{A'} < 3.5\,\mathrm{GeV}$ and $0.2\,\mathrm{GeV} < m_{h'} < 10.5\,\mathrm{GeV}$ in the exclusive searches and $1.1\,\mathrm{GeV} < m_{A'} < 3.5\,\mathrm{GeV}$ and $2.2\,\mathrm{GeV} < m_{h'} < 10.5\,\mathrm{GeV}$ in the inclusive scenario.

No significant signal above the expected Standard Model background was observed allowing to set limits in the parameters of the dark sector, as shown in fig. 50 [101]. In the assumption that $\alpha_D=1/137$ those results exclude the region $\epsilon^2>6.4\times10^{-7}$ for mass of the dark photon less than 1 GeV and mass of the dark Higgs less than 8 GeV. The backgrounds to these searches are very low and the results will scale almost linearly with the integrated luminosity which makes the future searches at Belle II very promising.

6'2.3. Search for dark Higgs at KLOE. KLOE2 collaboration searched for dark Higgs-strahlung process in the $e^+e^- \to A'h'$ process [100]. An assumption that h' is lighter than A' was made leading to a final state where only the A' decay products are seen and the events have missing energy signature since the lifetime of the dark Higgs boson would be so large that it would escape detection. This is the so-called "invisible" dark Higgs scenario. This scenario would be satisfied for example if the Higgs boson mass is of $O(100\,{\rm MeV})$ and $\alpha_D=\alpha_{\rm EM}$ then the lifetime of the dark Higgs would be $\tau_{h'}\approx 5\,\mu{\rm s}>\tau_\mu$ for $\epsilon=10^{-3}$.

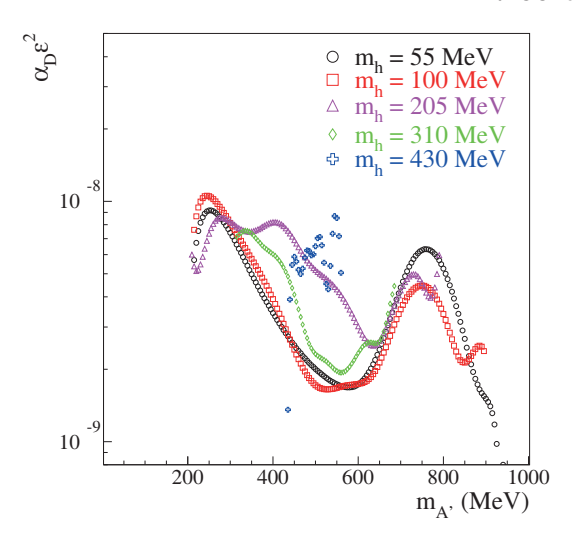


Fig. 51. – Excluded region with 90% C.L. with the KLOE-2 on-peak sample [100].

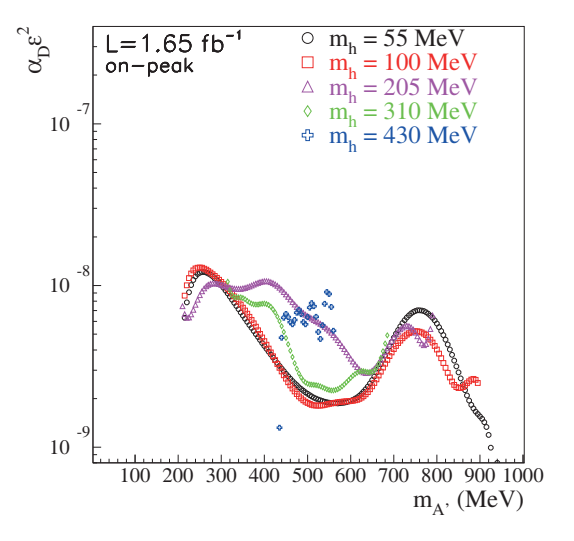


Fig. 52. – Off-peak exclusion limits at 90% C.L. [100].

Data analysis was performed on two samples of the e^+e^- centre-of-mass energy:1.65 fb⁻¹, at the ϕ peak ~ 1019 MeV (on-peak data) and 0.206 fb⁻¹ at energy of ~ 1000 MeV (off-peak sample). Only the $\mu^+\mu^-$ decay channel of the dark photon was studied limiting the sensitivity to $m_{A'} > 210$ MeV. The absolute value of the missing momentum was required to be more than 40 MeV.

After the application of the selection criteria and the calculation of the expected background no excess of events providing evidence for the dark Higgs-strahlung process was found. This allowed to place 90% confidence level Bayesian upper limits on the cross-section for the on-peak and off-peak samples separately. The results were converted in terms of $\alpha_D \epsilon^2$ and are shown in fig. 51 for the on-peak and in fig. 52 for the off-peak samples, where the excluded regions are for different values of $m_{h'}$.

7. – Conclusions and discussion

The dark photon physics attracted recent interest due to the possibilities it provides for the explanation of several phenomena at the same time —the muon anomalous magnetic moment, the possible indications for dark matter scattering signals in high purity experiments, the dark matter annihilation mechanism.

Grand Unification Models like for example SU(5), SO(10), string theories are with rich phenomenology and additional type of interaction usually appear naturally so it is difficult to imagine that any real unification could take place without extra gauge bosons. Some of them could be neutral and light, thus accessible even to present state-of-the-art experiments.

The present experimental results do cover a large area of the parameter space of the dark photons but most of them are specific to a given theoretical scenario. While we understand that a really general search with no *a priori* assumption is difficult, more model independent searches covering wider range of models are highly welcome. A wide panorama of new searches is foreseen in the next 5–10 years allowing to explore and constrain the parameter space of different models.

The discovery potential of this new generation of experiments can lead to observations which could redefine our understanding of nature.

* * *

The authors would like to thank Antonella Antonelli, Fabio Bossi, Paolo Valente, Matthew Moulson, Tommaso Spadaro and Maxim Pospelov for useful discussions. VK acknowledges partial support from University of Sofia under contract SU-FNI 57/2015.

REFERENCES

- [1] CMS COLLABORATION (CHATRCHYAN S. et al.), Phys. Lett. B, 716 (2012) 30.
- [2] ATLAS COLLABORATION (AAD G. et al.), Phys. Lett. B, 716 (2012) 1.
- [3] PLANCK COLLABORATION (ADE P. A. R. et al.), Astron. Astrophys., 571 (2014) A22.
- [4] AMS-02 COLLABORATION, Talks at the "AMS Days at CERN", 15-17 April 2015.
- [5] PAMELA COLLABORATION (ADRIANI O. et al.), Nature, 458 (2009) 607.
- [6] Fermi LAT Collaboration (Ackermann M. et al.), Phys. Rev. Lett., 108 (2012) 011103.
- [7] AMS COLLABORATION (AGUILAR M. et al.), Phys. Rev. Lett., 110 (2013) 141102.
- [8] Bernabei R. et al., Eur. Phys. J. C, 67 (2010) 39.
- [9] COGENT COLLABORATION (AALSETH C. E. et al.), arXiv:1401.3295 [astro-ph.CO].
- [10] Blum T., Denig A., Logashenko I., de Rafael E., Lee Roberts B., Teubner T. and Venanzoni G., arXiv:1311.2198 [hep-ph].
- 11] The G-2 Collaboration (Benett G. W. et al.), Phys. Rev. D, **73** (2006) 072003.
- [12] Particle Data Group (Olive K. A. et al.), Chin. Phys. C, 38 (2014) 090001.
- [13] LE DALL M., POSPELOV M. and RITZ A., arXiv:1505.01865 [hep-ph].
- [14] ESSIG R., JAROS J. A., WESTER W., ADRIAN P. H. and ANDREAS S. et al., arXiv:1311.0029 [hep-ph].
- [15] CHERRY J. F., FRIEDLAND A. and SHOEMAKER I. M., arXiv:1411.1071 [hep-ph].
- [16] OKUN L. B., Sov. Phys. JETP, **56** (1982) 502 (Zh. Eksp. Teor. Fiz., **83** (1982) 892).
- [17] HOLDOM B., Phys. Lett. B, **166** (1986) 196.
- [18] GALISON P. and MANOHAR A., Phys. Lett. B, **136** (1984) 279.
- [19] IZAGUIRRE E. and YAVIN I., arXiv:1506.04760 [hep-ph].
- [20] Andreas S., Niebuhr C. and Ringwald A., Phys. Rev. D, 86 (2012) 095019.
- [21] Alekhin S. et al., arXiv:1504.04855 [hep-ph].

- [22] Batell B., Pospelov M. and Ritz A., Phys. Rev. D, 80 (2009) 095024.
- [23] BILMIS S., TURAN I., ALIEV T. M., DENIZ M., SINGH L. and WONG H. T., arXiv: 1502.07763 [hep-ph].
- [24] Beda A. G. et al., arXiv:1005.2736 [hep-ex].
- [25] Bellini G. et al., Phys. Rev. Lett., 107 (2011) 141302.
- [26] Deniz M. et al., Phys. Rev. D, 81 (2010) 072001.
- [27] VILAIN P. et al., Phys. Lett. B, 302 (1993) 351; VILAIN P. et al., Phys. Lett. B, 335 (1994) 246.
- [28] Lee H. S., Phys. Rev. D, 90 (2014) 091702.
- [29] BATELL B., MCKEEN D. and POSPELOV M., Phys. Rev. Lett., 107 (2011) 011803.
- [30] Carlson C. E., Prog. Part. Nucl. Phys., 82 (2015) 59.
- [31] CARONE C. D., Phys. Lett. B, **721** (2013) 118.
- [32] An H., Pospelov M. and Pradler J., arXiv:1401.8287 [hep-ph].
- 33] FENG W. Z., SHIU G., SOLER P. and YE F., JHEP, 1405 (2014) 065.
- [34] GORBUNOV D., MAKAROV A. and TIMIRYASOV I., Phys. Rev. D, 91 (2015) 035027.
- [35] BJORKEN J. D., ESSIG R., SCHUSTER P. and TORO N., Phys. Rev. D, 80 (2009) 075018.
- [36] Beranek T. and Vanderhaeghen M., Phys. Rev. D, 89 (2014) 055006.
- [37] FAYET P., Phys. Rev. D, **75** (2007) 115017 (hep-ph/0702176 [HEP-PH]).
- [38] Blmlein J. and Brunner J., Phys. Lett. B, **731** (2014) 320.
- [39] Pospelov M., Phys. Rev. D, **80** (2009) 095002.
- [40] Endo M., Hamaguchi K. and Mishima G., Phys. Rev. D, 86 (2012) 095029.
- [41] AOYAMA T. et al., Prog. Theor. Exp. Phys., 2012 (2012) 01A107.
- [42] Hanneke D. et al., Phys. Rev. Lett., 100 (2008) 120801.
- [43] Mohr P. J. et al., Rev. Mod. Phys., 84(4) (2012) 1527-1605.
- [44] Rym Bouchendira et al., Phys. Rev. Lett., 106 (2011) 080801.
- [45] Brianna J. Mount, Matthew Redshaw and Edmund G. Myers, *Phys. Rev. A*, **82** (2010) 042513.
- [46] Sturm S. et al., Nature, **506** (2014) 467.
- [47] DAVOUDIASL H., LEE H. S. and MARCIANO W. J., Phys. Rev. D, 89 (2014) 095006.
- [48] D'Ambrosio G., Ecker G., Isidori G. and Portoles J., JHEP, 9808 (1998) 004.
- [49] BILMIS S., TURAN I., ALIEV T. M., DENIZ M., SINGH L. and WONG H. T., arXiv:1502.07763 [hep-ph].
- [50] Konaka A., Imai K., Kobayashi H., Masaike A., Miyake K., Nakamura T., Nagamine N. and Sasao N. et al., Phys. Rev. Lett., 57 (1986) 659.
- [51] RIORDAN E. M., KRASNY M. W., LANG K., DE BARBARO P., BODEK A., DASU S., VARELAS N. and WANG X. et al., Phys. Rev. Lett., 59 (1987) 755.
- [52] BJORKEN J. D., ECKLUND S., NELSON W. R., ABASHIAN A., CHURCH C., LU B., MO L. W. and NUNAMAKER T. A. et al., Phys. Rev. D, 38 (1988) 3375.
- [53] BROSS A., CRISLER M., PORDES S. H., VOLK J., ERREDE S. and WRBANEK J., Phys. Rev. Lett., 67 (1991) 2942.
- [54] DAVIER M. and NGUYEN NGOC H., Phys. Lett. B, 229 (1989) 150.
- [55] ALWALL J., HERQUET M., MALTONI F., MATTELAER O. and STELZER T., JHEP, 1106 (2011) 128.
- [56] CHARM COLLABORATION (BERGSMA F. et al.), Phys. Lett. B, 157 (1985) 458.
- [57] BERNARDI G., CARUGNO G., CHAUVEAU J., DICARLO F., DRIS M., DUMARCHEZ J., FERRO-LUZZI M. and LEVY J. M. et al., Phys. Lett. B, 166 (1986) 479.
- [58] GNINENKO S. N., Phys. Lett. B, **713** (2012) 244.
- [59] KLOE-2 Collaboration (Archilli F. et al.), Phys. Lett. B, 706 (2012) 251.
- [60] KLOE-2 COLLABORATION (BABUSCI D. et al.), Phys. Lett. B, 720 (2013) 111.
- [61] KLOE-2 COLLABORATION (BABUSCI D. et al.), Phys. Lett. B, 736 (2014) 459.
- [62] Anastasi A. et al., arXiv:1509.00740 [hep-ex].
- [63] WASA-AT-COSY COLLABORATION (ADLARSON P. et al.), Phys. Lett. B, 726 (2013) 187.
- [64] HADES COLLABORATION (AGAKISHIEV G. et al.), Phys. Lett. B, 731 (2014) 265.
- [65] Babar Collaboration (Lees J. P. et al.), Phys. Rev. Lett., 113 (2014) 201801.

- [66] BABAR COLLABORATION (AUBERT B. et al.), Phys. Rev. Lett., 103 (2009) 081803.
- [67] NA48/2 COLLABORATION (BATLEY J. R. et al.), Phys. Lett. B, 746 (2015) 178.
- [68] PHENIX COLLABORATION (ADARE A. et al.), Phys. Rev. C, 91 (2015) 031901.
- [69] APEX COLLABORATION (ABRAHAMYAN S. et al.), Phys. Rev. Lett., 107 (2011) 191804.
- [70] MERKEL H., ACHENBACH P., AYERBE GAYOSO C., BERANEK T., BERICIC J., BERNAUER J. C., BHM R. and BOSNAR D. et al., Phys. Rev. Lett., 112 (2014) 221802.
- [71] Batell B., Essig R. and Surujon Z., Phys. Rev. Lett., 113 (2014) 171802.
- [72] MINIBOONE COLLABORATION (DHARMAPALAN R. et al.), arXiv:1211.2258 [hep-ex].
- [73] WOJTSEKHOWSKI B., NIKOLENKO D. and RACHEK I., arXiv:1207.5089 [hep-ex].
- [74] RAGGI M. and KOZHUHAROV V., Adv. High Energy Phys., 2014 (2014) 959802.
- [75] IZAGUIRRE E., KRNJAIC G., SCHUSTER P. and TORO N., Phys. Rev. D, 91 (2015) 094026.
- [76] BABAR COLLABORATION (AUBERT B. et al.), arXiv:0808.0017 [hep-ex].
- [77] ESSIG R., MARDON J., PAPUCCI M., VOLANSKY T. and ZHONG Y. M., *JHEP*, **1311** (2013) 167.
- [78] BESIII COLLABORATION (ABLIKIM M. et al.), Phys. Rev. D, 87 (2013) 012009.
- [79] BNL-E949 COLLABORATION (ARTAMONOV A. V. et al.), Phys. Rev. D, 79 (2009) 092004.
- [80] ANELLI G. et al., CERN-SPSC-2005-013, CERN-SPSC-P-326.
- [81] HPS COLLABORATION (CELENTANO A.), J. Phys. Conf. Ser., **556** (2014) 012064 [arXiv:1505.02025 [physics.ins-det]].
- [82] Denig A., private communication.
- [83] VALENTE P., "High intensity electron beam and infrastructure", PADME kick off meeting, Frascati 20-21 April 2015, https://agenda.infn.it/contributionDisplay. py?contribId=12&confId=9280.
- [84] RAGGI M., "PADME dump", PADME kick off meeting, Frascati 20-21 April 2015, https://agenda.infn.it/contributionDisplay.py?sessionId=3&contribId=14&confId=9280.
- [85] ECHENARD B., ESSIG R. and ZHONG Y. M., JHEP, 1501 (2015) 113.
- [86] RAGGI M., KOZHUHAROV V. and VALENTE P., arXiv:1501.01867 [hep-ex].
- [87] Andreazza A. et al., Frascati Phys. Ser., 60 (2015) 1.
- [88] Balewski J. et al., A Proposal for the DarkLight Experiment at the Jefferson Laboratory Free Electron Laser, May 2012.
- [89] Balewski J. et al., arXiv:1412.4717 [physics.ins-det].
- [90] Freytsis M., Ovanesyan G. and Thaler J., JHEP, 1001 (2010) 111.
- [91] ALEXANDER J., "LDM search at Cornell", http://www.ge.infn.it/~ldma2015/ LDMA2015/Program.html.
- [92] BDX Collaboration (Battaglieri M. et al.), arXiv:1406.3028.
- [93] Andreas S., Donskov S. V., Crivelli P., Gardikiotis A., Gninenko S. N., Golubev N. A., Guber F. F. and Ivashkin A. P. et al., arXiv:1312.3309 [hep-ex].
- [94] JAEGLE I. (FOR THE BELLE/BELLE II COLLABORATIONS), talk given at "International Workshop on Baryon & Lepton Number Violation", 26-30 April (2015).
- [95] SHIP COLLABORATION (ANELLI M. et al.), arXiv:1504.04956 [physics.ins-det].
- [96] ALWALL J. et al., JHEP, **1407** (2014) 079.
- [97] ATLAS COLLABORATION (AAD G. et al.), JHEP, 1411 (2014) 088.
- [98] CMS COLLABORATION (KHACHATRYAN V. et al.), arXiv:1506.00424 [hep-ex].
- [99] Babar Collaboration (Lees J. P. et al.), Phys. Rev. Lett., 108 (2012) 211801.
- [100] KLOE-2 COLLABORATION (ANASTASI A. et al.), Phys. Lett. B, 747 (2015) 365.
- [101] Belle Collaboration (Jaegle I.), Phys. Rev. Lett., 114 (2015) 211801.